University of Glasgow
DEPARTMENT OF
AEROSPACE
ENGINEERING

Inviscid Modelling of Unsteady Flow Through Centrifugal Fans: Single Blade Passage Models

by

I Bennett and M Vezza

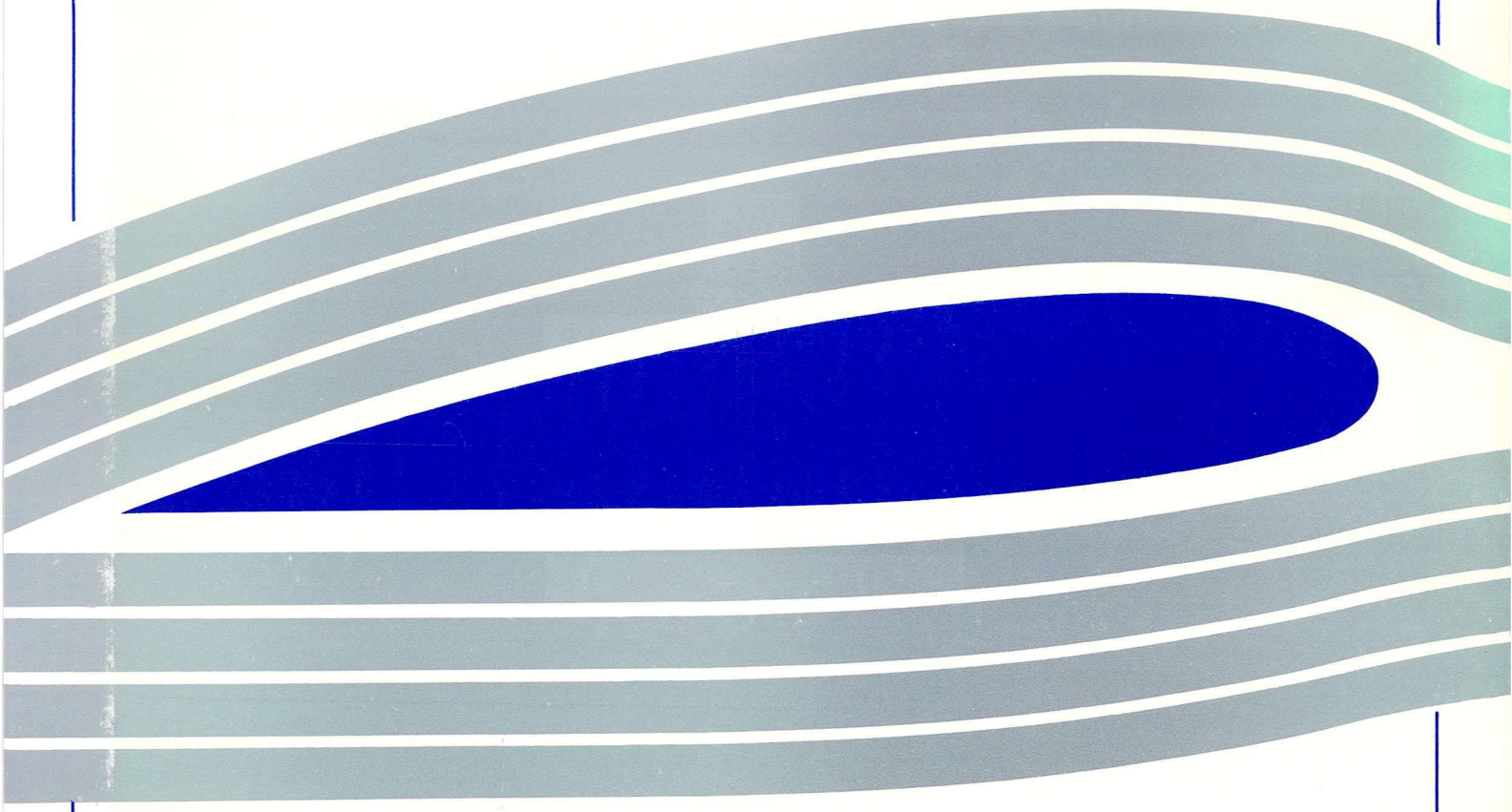

G.U. Aero Report No. 9309

Inviscid Modelling of Unsteady Flow Through Centrifugal Fans: Single Blade Passage Models

by

I Bennett and M Vezza

Department of Aerospace Engineering
University of Glasgow
G12 8QQ

Tel 041 330 4304

November, 1993.

Synopsis

The internal flows within two centrifugal blowers are examined using an inviscid formulation of the fluid equations of motion. The aim of the work was to predict the impeller unsteady stalled flow patterns whilst restricting the analysis to a single blade computational domain. Large stalled zones are predicted at flow rates corresponding to experiment. Some solver instabilities are reported for the most contorted computational meshes.

Contents

1. Introduction

The objective of this present work was to investigate whether an inviscid formulation of the equations of fluid motion could properly model highly stalled flow within centrifugal blade passages.

The earliest reference found, by the authors, to have used an inviscid method to model stalled flow within turbomachine blade passages was that of Stanitz [1948] . Stanitz, using a finite difference scheme to solve an inviscid flow formulation over a two dimensional blade-to-blade surface, was able to show pressure surface separation within a mixed flow impeller. It is interesting to note that Adler [1980] disputed the applicability of the Stanitz model, arguing that such separation would not occur if viscosity was properly modelled. However the need to model viscosity was later questioned by Bosman and Ahrabian [1984]. Using a 3D time-stepping inviscid Euler solver, Bosman and Ahrabian [1984] demonstrated not only recirculating regions but also localised unsteady velocity perturbations. The relative importance of the viscous terms in determining these gross flow features found within highly stalled flows has not been fully determined and it is to this end that the present research is aimed. This report only covers the first step of this research, that of using inviscid techniques; later the work will be extended to include viscosity. It should be noted that both Stanitz and Bosman used single blade passage models, to which this present work has been limited.

Without the generality of a multi-channel model, the authors accepted that they would not be able to demonstrate any of the asymmetric unsteady effects, namely that of rotating stall or a processional unsteady inlet vortex. Both of these phenomena have been experimentally detected, for example, by Soundra-Nayagam et al [1992]. Instead the authors hoped to gain some initial experience in applying CFD (Computational Fluid Dynamic) software to the much more simple single blade centrifugal fan models, gaining confidence and experience in model building, governing solution convergence and post -processing. In later work it was also envisaged to use this experience to help model the more computationally demanding multi-channel domains, the results from which will be used to highlight the applicability of the simplified single blade approach.

In order to verify the applicability of the techniques employed, two out of the three fan geometries examined here are compared against aerodynamic experimental tests completed by Bennett and Watson [1992].

A review of the fan modelling techniques is given in Bennett and Vezza [1992].

2. The Computational Models

For this work, instead a using valuable effort developing a customised CFD code, two commercial packages called PHOENICS and FLUENT were utilised. Both incorporate similar solution algorithms which are able to solve a variety of transport equations simultaneously. Indeed only a small portion of the total modelling capability of these codes was required to employ the full Euler equations.

In all three computational meshes were examined. The first model was a recalled library case demonstration PHOENICS model. Strictly speaking this was a high speed radial impeller rather than a centrifugal fan. Despite this, as a first tentative investigation into using such commercial codes, it proved a valuable and worthwhile introduction. Indeed several useful observations were noted.

The subsequent two models investigated were of an industrial centrifugal fan called the L3R. The computational meshes for these were constructed using a general mesh pre-processor called PATRAN, and then imported in FLUENT. These two cases represent the bulk of the work reported here. For the most sparsely meshed of these, a fully Unsteady Euler solution was computed.

Using the commercial codes, the Euler solution was not found in one computational run due to experienced stability problems. Instead the solutions were sought via a series of simplified steps. See Figure 1.

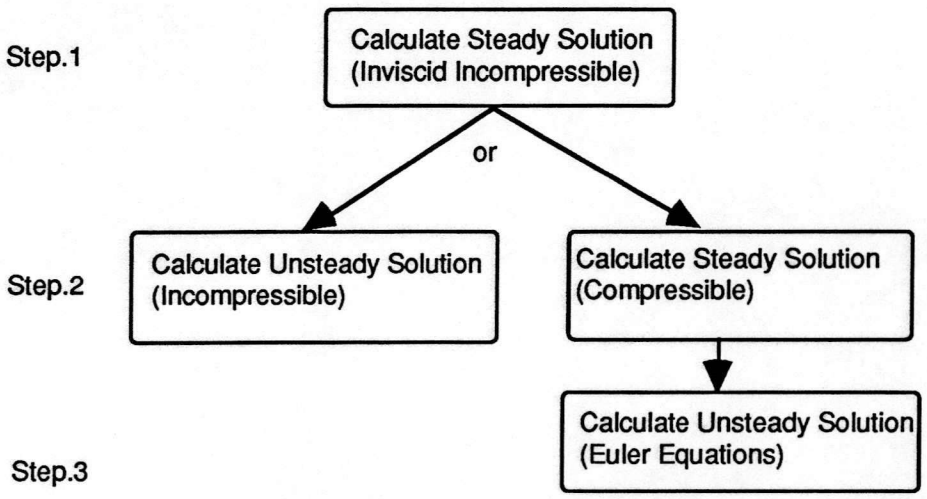

Figure 1 Steps to an Unsteady Solution

The left hand side of the above diagram represents the path to gain a solution to the incompressible formulation of the Euler equations, with the right hand side the path for the compressible equivalent.

The Unsteady Euler Equations, referred to a steadily rotating frame of reference, are as follows (Hirsch [1990]):

Conservation of Mass

$$\frac{\partial}{\partial t}\iiint_{\Omega}\rho d\Omega + \oiint_{S}\rho\vec{w}.d\vec{S} = 0 \qquad -(1)$$

Conservation of momentum

$$\frac{\partial}{\partial t}\iiint_{\Omega}\rho\vec{w}d\Omega + \oiint_{S}(\rho\vec{w}\otimes\vec{w} + pI).dS = -\oiint_{\Omega}\rho[2\vec{\omega}\times\vec{w} + \vec{\omega}\times(\vec{\omega}\times\vec{r})]d\Omega \qquad -(2)$$

Conservation of Energy

$$\frac{\partial}{\partial t}\iiint_{\Omega}\rho E d\Omega + \oiint_{S}(\rho\vec{w}I - k\nabla T)d\vec{S} = 0 \qquad -(3)$$

where the terms are defined

$$E = e + \frac{\vec{w}^2}{2} - \frac{\vec{u}^2}{2}$$

$$\vec{u} = \vec{w}\times\vec{r}$$

$$I = h + \frac{\vec{w}^2}{2} - \frac{\vec{u}^2}{2}$$

E = stagnation internal energy
I = rothalpy
w = velocity relative to rotating frame

(Note: the **I** term in the momentum equation is the matrix identity *not* rothalpy)

Therefore to solve the Unsteady Euler Equations ('step 3'), equations (1), (2) and (3) must be satisfied.
As already described the initial simplified computer models used only a steady incompressible formulation of the above equations. The incompressibility simplification makes the energy equation redundant, reducing the dimensions of the

problem by one. Consequently, only the first two equation sets, namely continuity and momentum require solving. i.e..

Conservation of Mass

$$\oiint_S \rho \vec{w}.d\vec{S} = 0 \qquad -(4)$$

Conservation of momentum

$$\oiint_S (\rho \vec{w} \otimes \vec{w} + pI).dS = -\iiint_\Omega \rho[2\vec{\omega} \times \vec{w} + \vec{\omega} \times (\vec{\omega} \times \vec{r})]d\Omega \qquad -(5)$$

together with constant ρ.

The above are the equations required for 'step 1'.

Once these were solved, compressibility was then introduced. This involved the introduction of Energy equation (3). Finally the additional time dependent terms were included for the unsteady runs.

The series of CFD runs completed are described in detail in the next three sub-sections, namely 2.1, 2.2 and 2.3. The first describes the PHOENICS Mizuki model runs. The second, the bladed and unbladed L3R FLUENT model runs. The third, the runs completed when the PHOENICS Mizuki model geometry was imported into FLUENT and rerun.

2.1 PHOENICS Mizuki model

Edwards [1985] constructed a PHOENICS CFD model of the Mizuki [1974] high speed centrifugal compressor and verified the predicted flow against Mizuki's experimentally measured velocities. In particular Edwards examined design and 25% greater than design, flow rates. This 'Mizuki Impeller' model, stored as a PHOENICS test case [PHOENICS Library No. 524], was recalled and used here as a first attempt to model highly stalled flow. The resultant flow fields calculated were similar to those presented by Bosman [1984] with large stall cells apparent at the low flow rates corresponding to rotating stall.

2.1.1 MIZUKI impeller Model Details

The computational model of the 12 bladed MIZUKI impeller library case was fully 3D and the equations solved were steady state, viscous (a high constant laminar viscosity that was characteristic of turbulent flow was used) and incompressible. Momentum source terms modelled the additional body forces needed for working within a rotating frame of reference. An inlet velocity condition prescribed the impeller mass flow and the air discharged through a constant pressure outlet positioned downstream of the impeller exit on a surface representative of the vaneless diffuser discharge.

The computational grid of 5 x 5 x 12 included cyclic boundary conditions at the segment edges of the vaneless space. Figure 1 shows the computational mesh used which represents one of the 12 blade passages.

2.1.2 Operating Conditions

Runs with flow coefficients of 0.4, 0.2 and 0.1 were completed, the former representing design flow. The impeller rotated at 6000 rpm in all model runs.

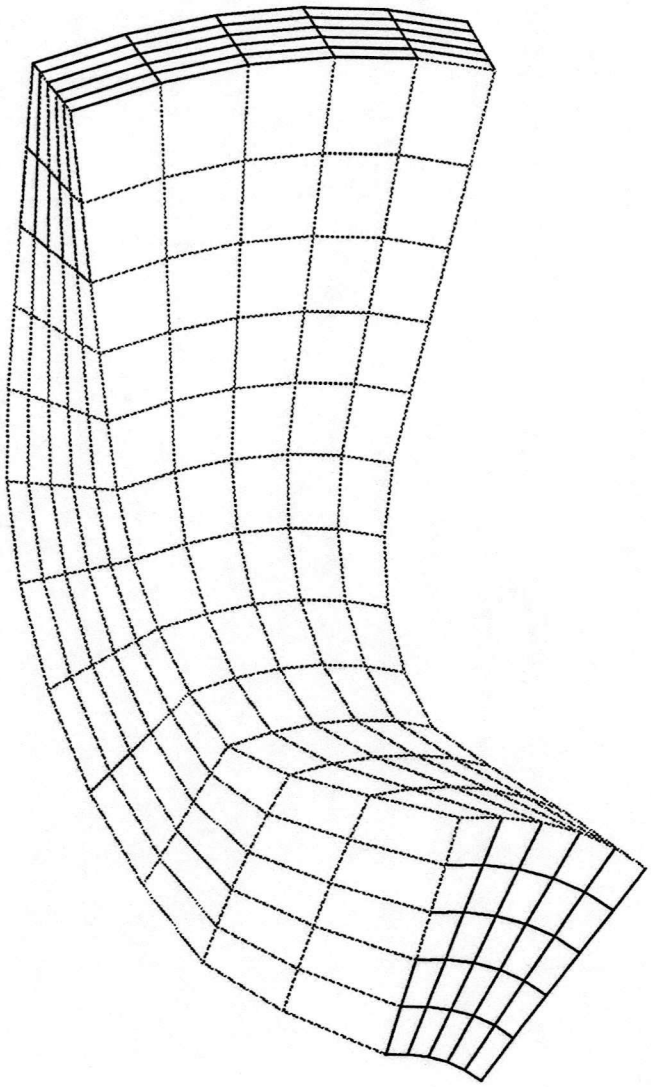

Figure 2 *MIZUKI impeller finite volume computational mesh*

2.1.3 Results

The most significant computational investigations are reported here designated by the file names used for computer storage. Tabulated below are their salient features.

Table 1 PHOENICS Mizuki impeller computer runs

Model Name	Flow Coeff	Viscosity	Solver	Error *E8	Comments
MizA	0.4	Turbulent (constant)	False Time step	≈ E2	Standard Library Run
MizB	0.4	Inviscid	False Time step	≈ E2	Without viscosity the results were the same as MizA
MizC	0.1	Inviscid	False Time step	≈ E5	Large areas of recirculating flow
MizD	0.2	Inviscid	False Time step	≈ E7	Some small areas of recirculation
MizG	0.4	Inviscid	Linear	≈ E2	No difference in convergence time or final residual errors over MizB due to Linear solver
MizI	0.1	Inviscid	Linear	≈ E6	Large recirculating flow as shown by MizC.

Observations are noted below:

2.1.3.a Effect of viscosity on solution

There is no noticeable difference between the solutions of models MizA and MizB and it is concluded that viscosity has very little influence on the velocity and pressure fields within the Mizuki impeller when operating at design conditions.

$\varphi = 0.4 \rightarrow$

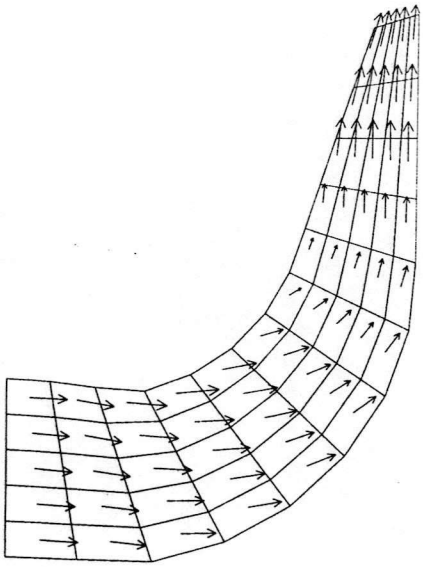

$\varphi = 0.2 \rightarrow$

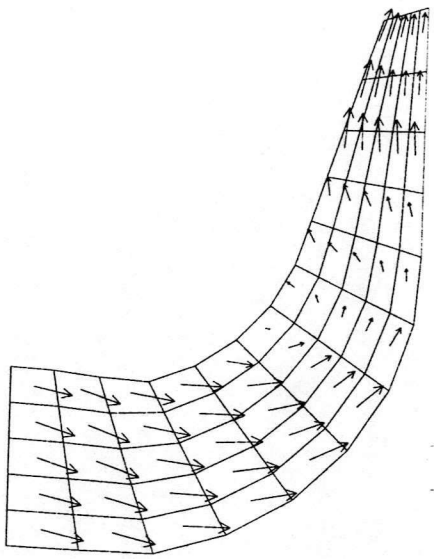

$\varphi = 0.1 \rightarrow$

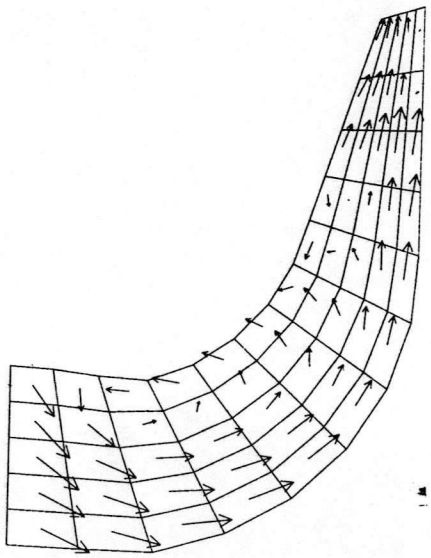

2.1.3.b Flow redistribution due to variations in flow coefficient

As the flow rate is reduced there an emergence and subsequent growth of recirculating eddies. Figure 3 shows the development using relative (to the impeller rotation) velocity vectors of the flow on plane adjacent to the blade pressure surface. Most prominent is the reverse flow at the impeller inducer. This flow is similar to that predicted by Bosman [1984] (see Figure 4). However unlike Bosman [1984] the large recirculation is displayed on the pressure, rather than the suction surface.

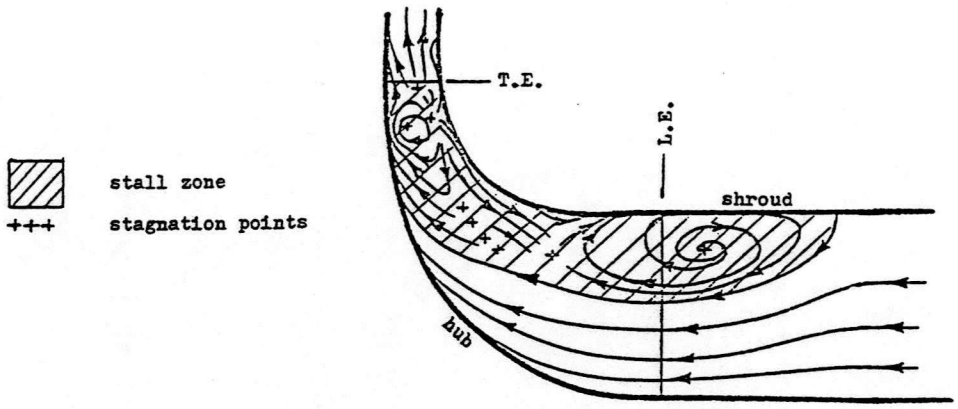

Figure 4 Recirculation on the suction surface Predicted by Bosman [1984]

The three meridonial planes of velocity vectors, shown in Figure 5, are from the MizI model run and reveal the extent and three dimensional nature characteristic of such highly stalled flows.

It is not only the velocity distribution that is effected by low volume flow rate. Significant qualitative variations in pressure occur as may be seen in Figure 6. Notice how for the design case the pressure contours are almost normal to the velocity vectors; however for the low flow case the pressure contours stratify so that the maximum pressure gradient is in the radial direction. This is particularly apparent just after inlet, near the shroud.

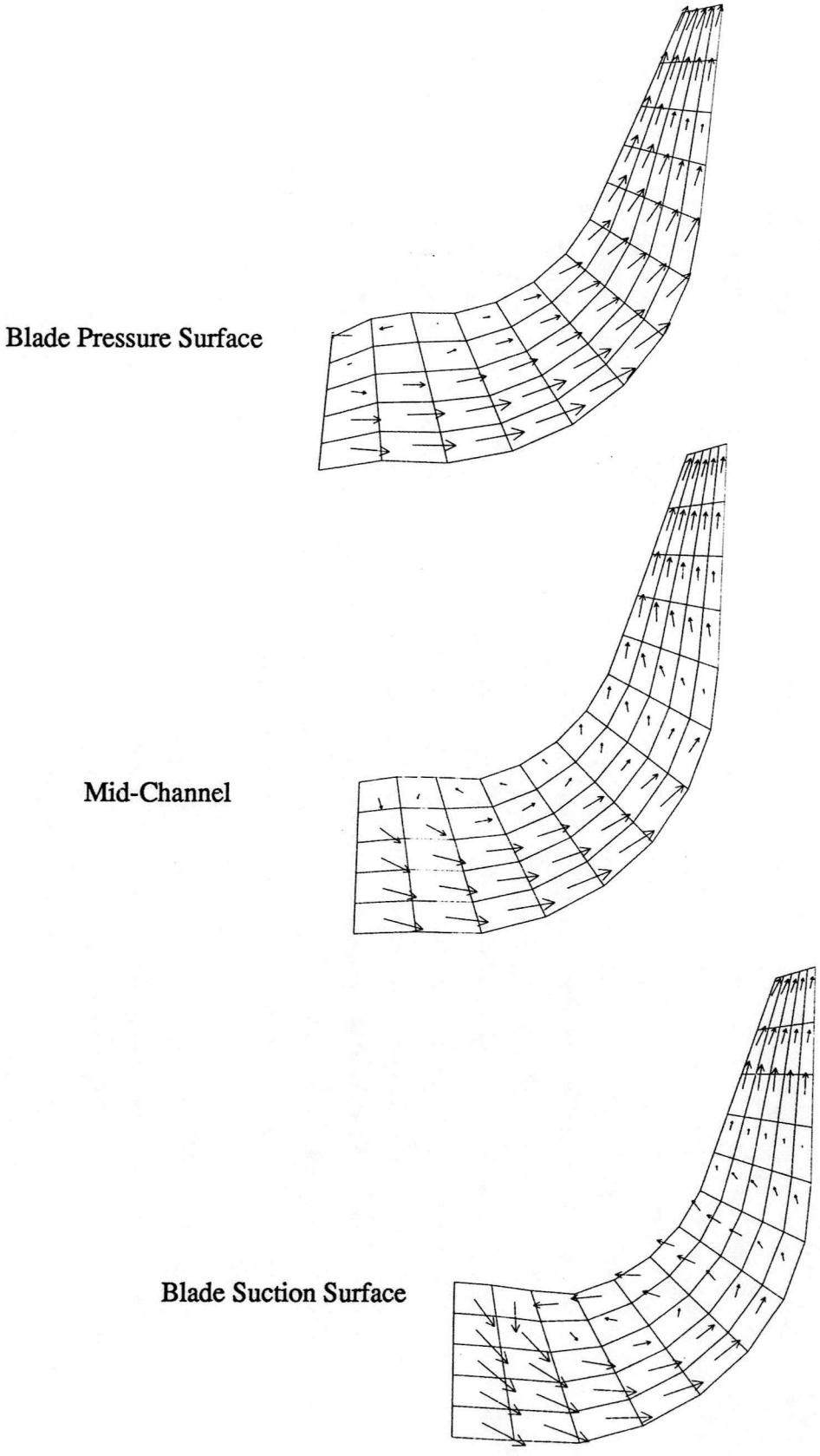

Figure 5 The Three Dimensional Nature of Highly Stalled Impeller Blade Passage Flow: Velocity Vectors

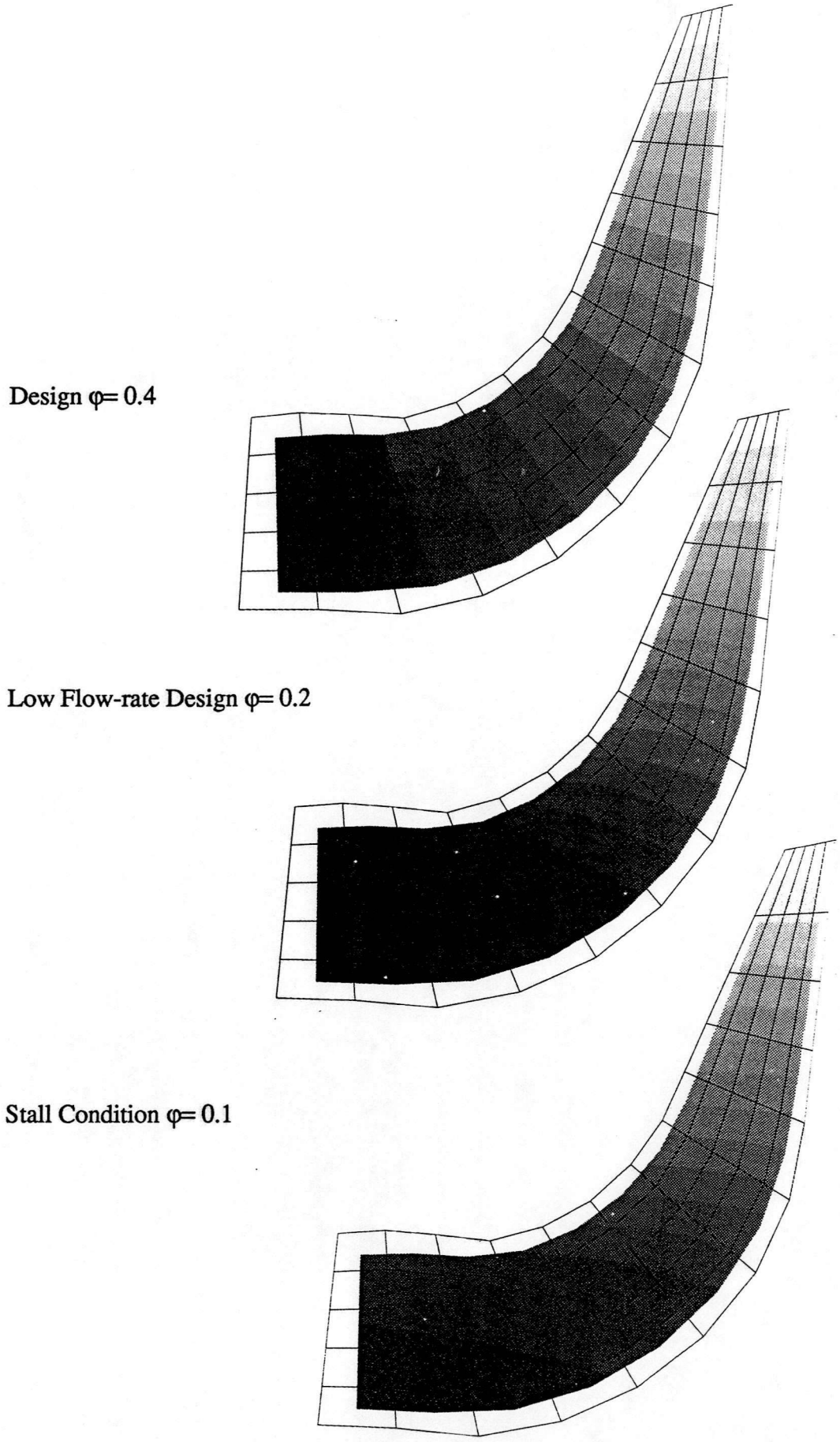

Figure 6 Variation in pressure distribution with changes in flow rate

2.1.3.c Solution stability and convergence

PHOENICS uses an iterative solution procedure to 'solve' the governing equations for which the user must define the convergence. For the MIZUKI impeller investigation the magnitude of the error residuals, reported by PHOENICS every iteration, were used to gauge when to stop the program. The accepted magnitudes of the error residuals were set by the levels recorded for the standard design flow model test case, MIZA.

Using this approach it quickly became apparent that as the flow coefficient was lowered the problem became less stable and larger numbers of iterations were necessary to gain the convergence quantified by the standard run. As an indication of this, for the design flow cases approximately 150 iterations were required; for the highly stalled flow it became necessary to increase this to 500 iterations. Future iterations beyond this were not effective in reducing the larger residual errors which appeared when modelling low flow rates, and consequently the desired residual levels were not always achieved.

2.2. Single Blade Passage Models of the L3R impeller using FLUENT

2.2.1 Introduction

Two models of the L3R centrifugal fan impeller were constructed. The main differences between them are shown below in Table 2.

Table 2 L3R model differences

Model	Number of Computational cells	Blade Thickness Modelled?
1 (bladed)	12x10x41= 4920	Yes
2 (unbladed)	5x5x30= 750	No

These models will be subsequently referred to as the *'bladed'* and *'unbladed'* cases, for which the computational grids are shown if Figure 7. The reasons why two different computational meshes were built for the same impeller are explained below.

2.2.1.a Choice of computational domain

When constructing the mesh for a single blade passage sector of an impeller the blade boundary may be placed within or at the edges of the computational domain.

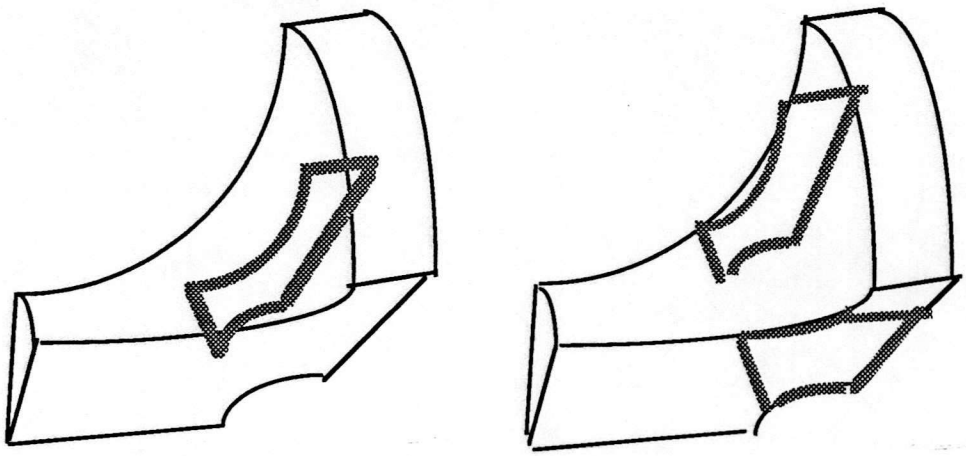

Figure 7 *Blade modelled within and alternatively at the edge of the computational grid*

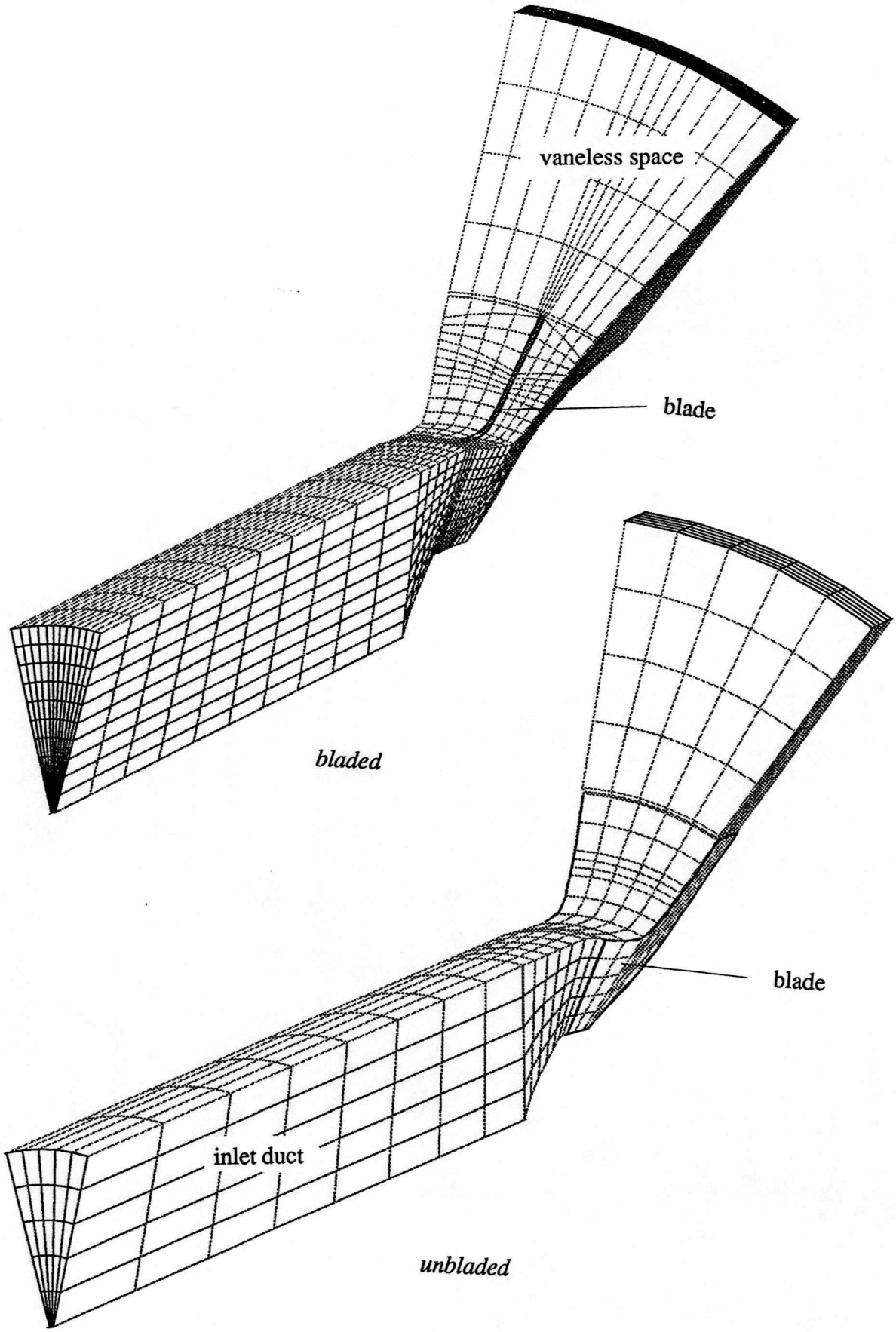

Figure 8 L3R Impeller Computational Meshes

When using FLUENT physical walls must be modelled 2 cells thick for correct implementation of the boundary conditions. For a densely meshed model, together with the restraint of a structured grid, this addition can mean a significant increase in the number of required cells particularly when the plane on which the cell dimensions are to be increased is perpendicular to the direction in which the number of cells is the greatest. This worst scenario appears when attempting to model highly stalled impeller flow where the careful application of boundary conditions are required. For uniform inlet and discharge boundaries to be appropriate in these cases, a significant proportion of the flow upstream and downstream of the impeller must be modelled, as the unsteady disturbances influence the flow several duct diameters away from the impeller. Despite the expected extension in computer run times due to the increased number of computational cells, this type of model was built first , as it would allow progression to a multi-channel model where the modelling of blade thickness would be necessary. It is referred to as the *bladed* L3R model in the remaining text. This configuration is shown at the top of Figure 8. The other drawing in Figure 8 is the *unbladed* model. The 'bladeless' simplification was justified as the impeller blade plate thickness caused little blockage within the L3R fan. A significant saving in computation cells was made, with the blade passage bounded cyclically by wall boundaries, as shown in Figure 8, representing the impervious blade surfaces. Apart from the savings in computer run times due to the reduction in the number of cells, this approach had advantages in grid construction as the model was axisymmetric: once a meridonial surface was constructed it could be simply rotated to form the full computational three dimensional domain.

2.2.1.b The Equations Solved by FLUENT

The initial simplified computer models used only a steady incompressible formulation of the Euler equations. All these simplifications made the energy equation redundant, reducing the dimensions of the problem by one. As such only the first two equation sets, namely continuity and momentum required examination. i.e..

Conservation of Mass

$$\oiint_S \rho \vec{w}.d\vec{S} = 0 \qquad -(4)$$

Conservation of momentum

$$\oiint_S (\rho \vec{w} \otimes \vec{w} + pI).dS = -\iiint_\Omega \rho[2\vec{\omega} \times \vec{w} + \vec{\omega} \times (\vec{\omega} \times \vec{r})]d\Omega \qquad -(5)$$

together with constant ρ.

Once these were solved, compressibility was then introduced. This involved the re-introduction of Energy equation. Finally the additional time dependent terms were included for the unsteady runs.

2.2.1.c Boundary Conditions

The choice of appropriate boundary conditions for the isothermal steady-flow problems include:

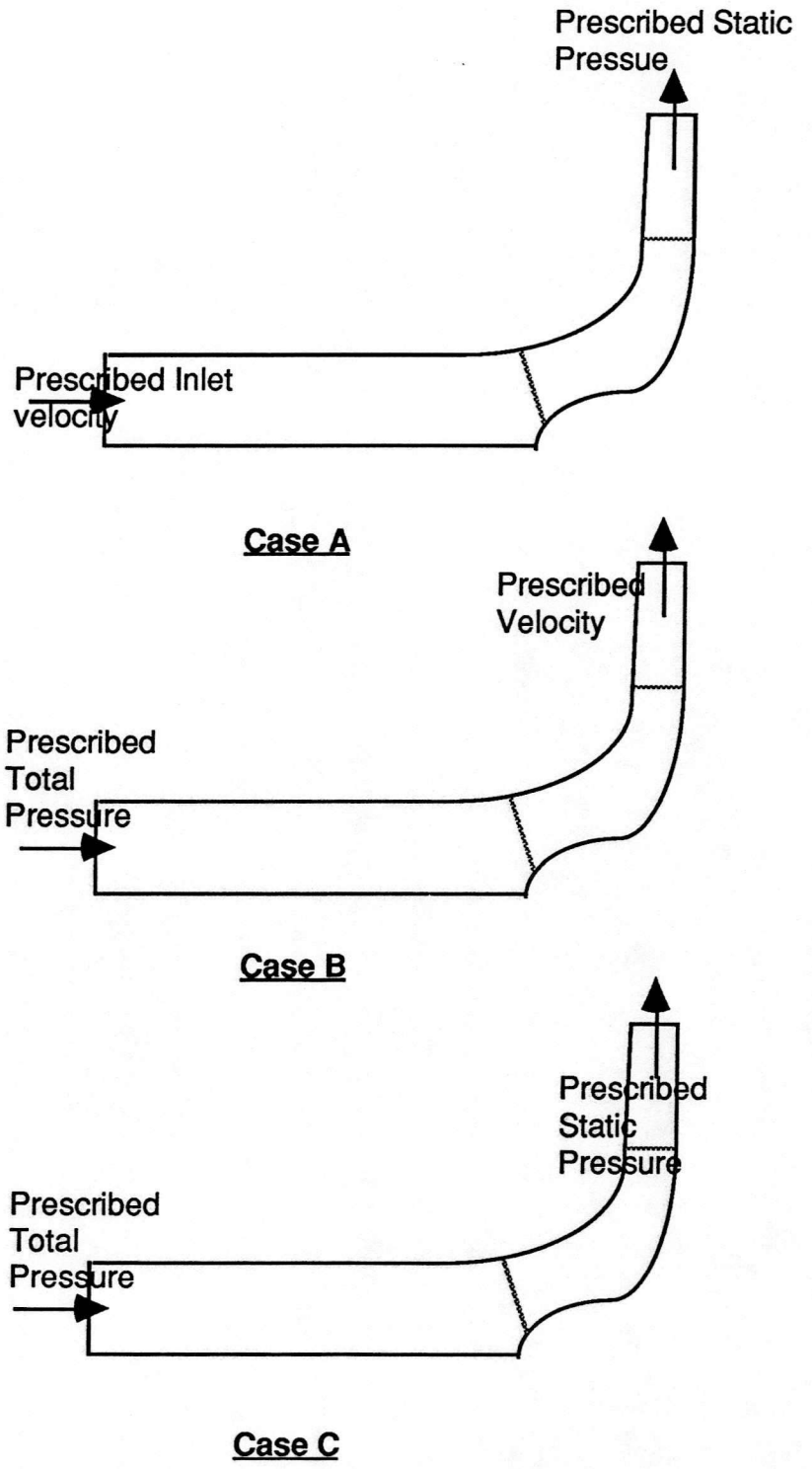

Figure 9 Isothermal Steady Flow Boundary Conditions

Boundary type A was chosen as appropriate measurements were taken at these boundaries during the aerodynamic experimental testing (Bennett and Watson [1992]). We should also note that Case C, despite knowing these boundary pressures, it was not though an appropriate choice as the computational model would not induce the correct inlet mass flow. It was considered that a prescribed inlet velocity would predict a more realistic velocity field within the blade passages, than a prescribed pressure rise across the inlet and discharge boundaries. For the runs involving the Energy equation, temperature was additionally prescribed at the fan inlet and discharge. The switch to time dependency did not necessitate a change in boundary conditions.

2.2.1.d Convergence Criteria

Although FLUENT by default reports the complete field residual errors, the most useful and indicative means found to gauge convergence was to examine the calculated pressure field at inlet. These values were examined against iterations to see if they settled to a constant value: once attained, the solution was deemed converged. The two L3R computer models are now discussed in term. The objective of these runs was to examine highly stalled flow within the blade passages.

2.2.2 Single Passage L3R *Bladed* Model Runs

This section describes the runs completed using the L3R bladed model.

2.2.2.a Solution strategy

The FLUENT documentation warns that the programs SIMPLE (Semi-Implicit-Pressure-Linked-equations) solver employed is not entirely suitable for solving highly swirling flows or flows with non-linear pressure gradients. Unfortunately it is in the nature of centrifugal compressors to operate within both of these regimes and it was therefore anticipated that some stability problems would occur.

The adopted solution strategy was based around reducing the affect of pressure on the problem. It involved the application of flow boundaries representative of the high-flow/low-pressure operating regime of the fan, and hence making the convective momentum terms outweigh the diminished pressure-gradient terms. In this way the model would initially be of a fan operating without any system resistance, then with prescribed step decrements in inlet flow velocity, the fan would develop higher and higher pressures finally reaching the stall condition sought. It was thought that this approach of steadily increasing the pressure gradient would have a beneficial effect on stability. In practice however, this approach did not overcome the numerical instabilities and after a series of exploratory runs the model was abandoned. Despite these negative results, the attempts are documented here to act as 'negative research' .

2.2.2.b Model Set-up

The prescribed operating conditions used in the preliminary runs represented the fan theoretical maximum flow i.e. when the fan static pressure rise was zero. The coriolis and centrifugal body forces were set to model the impeller rotating at 1118 rpm, for it was at this velocity that the experimental flow measurements were taken by Bennett and Watson [1989].

Non-slip boundaries rather than slip boundaries, that are normally prescribed for inviscid flow, were used on the blade, hub and shroud surfaces. This seemingly ill-prescribed boundary set was acceptable as the influence of these boundaries on the inviscid flow field was uncoupled by a prescribed low (negligible) constant laminar viscosity of 1×10^{-15} kg/msec. Checks carried out, before impeller model implementation, on parallel wall test cases confirmed that this uncoupling did indeed occur.

2.2.2.c History of Computer Runs

The pertinent runs completed using the L3R bladed model are shown below in Figure 11. The maximum inlet volume flow boundary was applied in all cases apart from the last 3 runs.

2.2.2.d Description of the bladed L3R model computer runs

In order to fully understand the reasons behind each model run, all of the above tabulated examples in Table 3 are examined in turn.

The first of the these, L3RT, followed on from several exploratory computer runs that are not individually documented here. These early runs, although showing numerical stability, were not able to yield fully converged solutions and it became apparent that some tuning of the solution parameters would be required. It is the effect of changing these parameters on the model stability and convergence that is the main concern here. These 'solution parameters' are user defined solution controls called 'relaxation parameters' and 'numbers of sweeps' . These may be independently changed for each variable, namely the three velocities and pressure for the inviscid incompressible runs.

The first three runs, namely L3RT, L3RX and L3RY, were all experiments to investigate reductions in the relaxation parameters. Of these the only positive result came from L3RX, in which the step drop in relaxation parameters triggered a step drop in pressure error residual. However, this positive result was marred due to a trade off in increased velocity residuals . The pressure and velocity residuals plots for run L3RX are shown below in Figure 10.

When reading Table 3, "600+900" in the 'number of iterations column' means that after 600 of the scheduled 1500 iterations the switch in relaxation parameters was made. The effect of such a step change can be seen in Figure 10.

Table 3 Bladed Model L3R Fluent Runs

	Relaxation Parameters		No. of Sweeps			Residual Values				Comments
Run Filename	Pressure	Velocity	Press.	Vel.	No. of iters	Press.	U-Vel	V- Vel	W-Vel	
L3RT	0.4/0.2	0.3/0.1	20	10	500 +1000	$5x10^{-3}$	$4x10^{-3}$	$7x10^{-3}$	$2x10^{-3}$	Some divergence of the velocity terms after change in relaxation parameters
L3RX	0.3/0.1	0.2/0.05	15	10	600 +900	$3x10^{-3}$	$3x10^{-3}$	$5x10^{-3}$	$1x10^{-3}$	Large drop in pressure residuals but some divergence of the v-velocity residuals.
L3RY	0.05/0.02	0.05	15	10	75+75	$5x10^{-3}$	$3x10^{-3}$	$5x10^{-3}$	$1x10^{-3}$	Investigating the effect of a change in pressure relaxation. Small increase in pressure residuals. No change in velocities.
L3RZ	0.02	0.05	20	10	30	$5x10^{-3}$	$3x10^{-3}$	$5x10^{-3}$	$1x10^{-3}$	Investigation to see if increasing the number of sweeps on pressure made any difference. Results showed no change.
L3RBB	0.4	0.3	30	10	200	$7x10^{-3}$	$1x10^{-3}$	$1x10^{-3}$	$1x10^{-3}$	First time that Variable History records were taken during a run. Interesting results showed oscillations in pressure at inlet.
L3RCC	0.4	0.3	30	10	500	$6x10^{-3}$	$9x10^{-4}$	$1x10^{-3}$	$8x10^{-4}$	This run was a continuation of L3RBB
L3REE	0.4	0.3	50	10	300	$1x10^{-2}$	$2x10^{-3}$	$2x10^{-3}$	$1x10^{-3}$	Both this run and the one following were investigations into the changes in the number of pressure sweeps.
L3RFF	0.4	0.3	50	10	300	$1x10^{-2}$	$2x10^{-3}$	$3x10^{-3}$	$3x10^{-3}$	This run seemed to deviated from the predicted pressure values expected from viewing L3RCC variable History plots.
AL3RB	0.4	0.3	30	10	500	$9x10^{-3}$	$2x10^{-3}$	$2x10^{-3}$	$1x10^{-3}$	Continuation of L3RCC
AL3RD	0.4	0.3	30	10	500	$1x10^{-2}$	$2x10^{-3}$	$2x10^{-3}$	$1x10^{-3}$	As test , with new boundary
AL3RF	0.075	0.3	30	10	500	$2x10^{-2}$	$2x10^{-3}$	$3x10^{-3}$	1x10-3	See Fig. 14
AL3RH	0.2	0.15	30	10	500	$3x10^{-3}$	$1x10^{-3}$	$1x10^{-3}$	$1x10^{-3}$	See Fig. 14
AL3RI	0.4	0.3	30	10	250	$1x10^{-2}$	$2x10^{-3}$	$2x10^{-3}$	$2x10^{-3}$	See Fig. 14
AL3RJ	0.2	0.15	30	10	1000	$4x10^{-3}$	$2x10^{-3}$	$2x10^{-3}$	$2x10^{-3}$	See Fig. 14
AL3RL	0.1	0.075	30	10	1000	$2x10^{-3}$	$1x10^{-3}$	$2x10^{-3}$	$1x10^{-3}$	See Fig. 14
AL3RM	0.4	0.3	30	10	500	$3x10^{-2}$	$3x10^{-3}$	$4x10^{-3}$	$2x10^{-3}$	See Fig. 14
L3RBBB	0.4	0.3	30	10	750	$4x10^{-2}$	$3x10^{-3}$	$4x10^{-3}$	$1x10^{-2}$	This run had the inlet velocity field reduced from a uniform $43.9ms^{-1}$ to $35ms^{-1}$. We were looking for an improvement in convergence. After about 300 iterations problem started to diverge.
L3RDDD	0.1	0.3	30	10	500	$1x10^{-1}$	$3x10^{-3}$	$7x10^{-3}$	$7x10^{-3}$	The above run was restarted with a smaller pressure relaxation parameter to see if it would prevent the divergence. This first attempt showed some unstable trends. The next run confirmed divergence.
L3REEE	0.1	0.3	30	10	400	$5x10^{-2}$	$3x10^{-3}$	$6x10^{-3}$	$6x10^{-3}$	Continuation of the previous run.

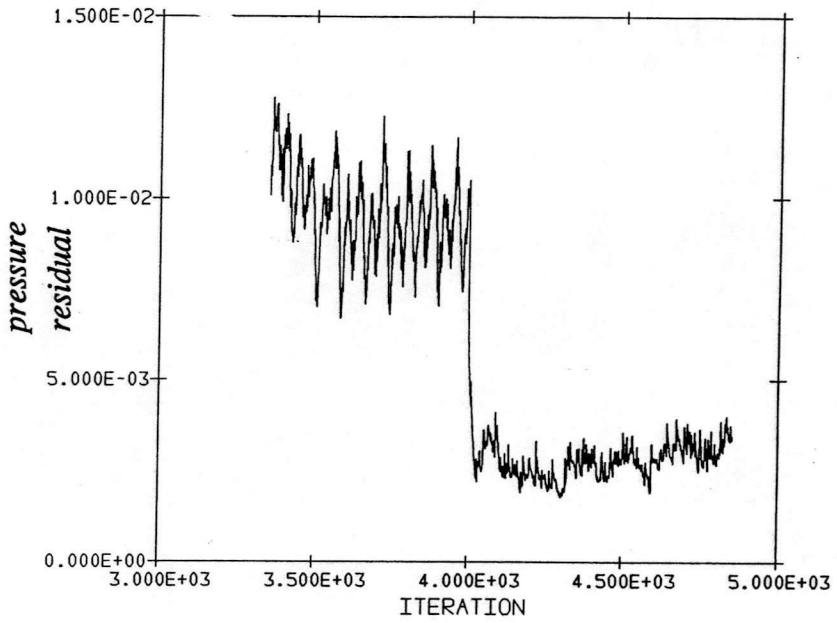

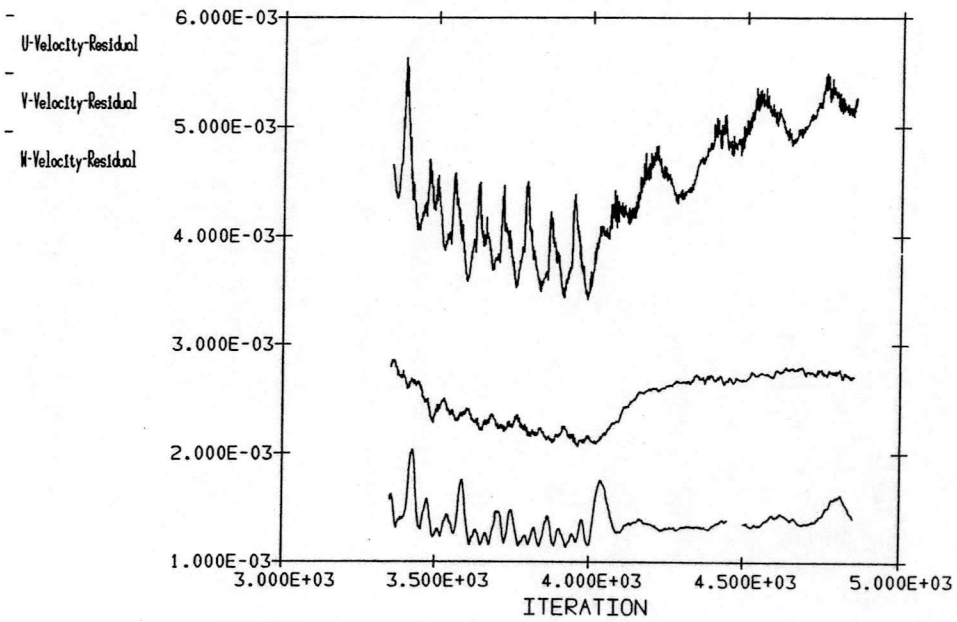

Figure 10 Plot of pressure and velocity residuals for run L3RX

Run L3RY that followed was an attempt to see if the velocity and pressure values could be uncoupled by changing only the pressure relaxation parameter. This was unsuccessful as there was an increase in pressure error residuals.

During the execution and analysis of the preceding runs it became increasingly apparent that the reported residual errors were not sufficient to determine the solver performance i.e. just how quickly, if at all, the equation set was converging. It became necessary to invoke FLUENT's variable history option. This utility records, after each solution iteration, velocity and pressure magnitudes at any user specified location within the domain. Consequently the solution may be said to have converged, for a steady state run, when these reported variable histories settle to constant values.

For the remaining runs in the section it was decided to record the pressure field at the inlet of the domain, with these values used to determine convergence.

Using FLUENT's variable history utility, the model was restarted with the more conventional, that is FLUENT's default , values for pressure and velocity relaxations of 0.4 and 0.3 respectively. This model run was successful and was continued for another 500 iterations finally being stored as L3RCC. A variable history plot which includes run L3RCC is show in Figure 11.

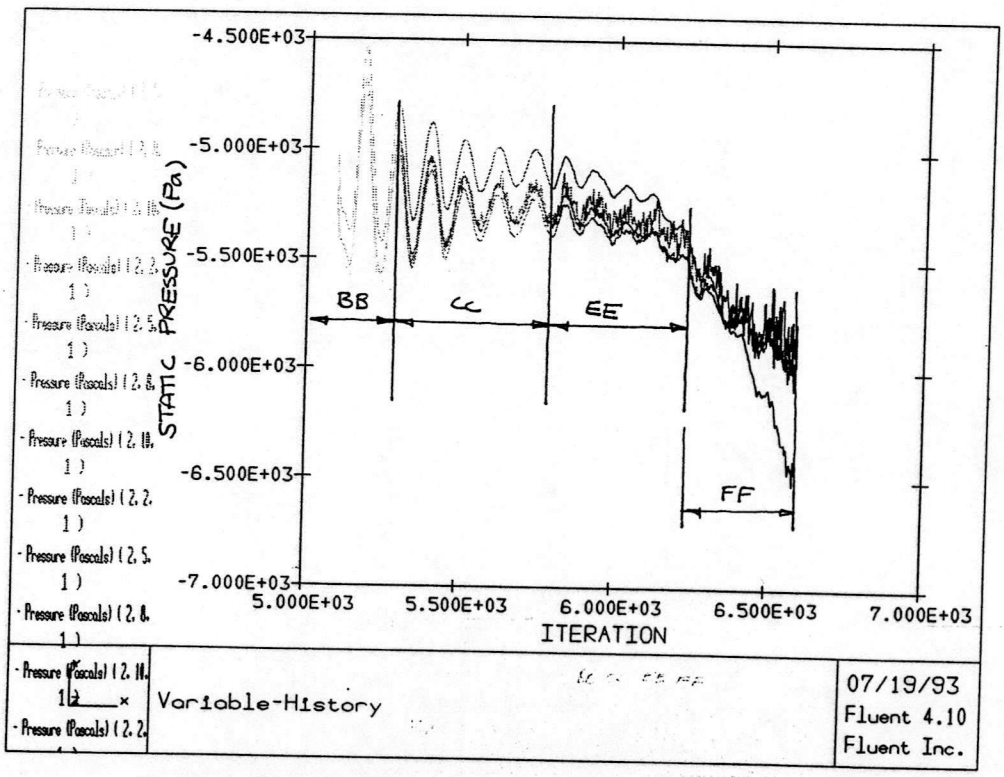

Figure 11 Variable History Plot of Pressure at Inlet

As can be seen in Figure 11 the amplitude of oscillation for run L3RCC was decreasing with iteration, suggesting that the problem was approaching convergence. The number of pressure sweeps was further increased from 30 to 50 in order to aid the damping process (runs L3REE and L3RFF). However instead of the problem settling to a constant value, the pressure at inlet drifted away from the projected mean settling value. At this point it was concluded that 30 pressure sweeps should be used for all further runs as it was thought that using 50 sweeps could cause instabilities. However in runs that followed, this was shown to be an incorrect deduction.

This method of putting computer runs nose-to-tail produced rapid results but did not clearly show the effect of each individual solution parameter. Indications were clouded by the influence of the initial field data set ,which in previous runs had shown, could even effect the overall stability of the solver. It was decided therefore, in order to ensure fair comparisons, that the jobs would be run in parallel. These runs, starting with the same initial data set, and would differ only by a single solution parameter.

Because of the complex relationships connecting each of the runs in this investigation, a tree diagram is drawn below to aid understanding.

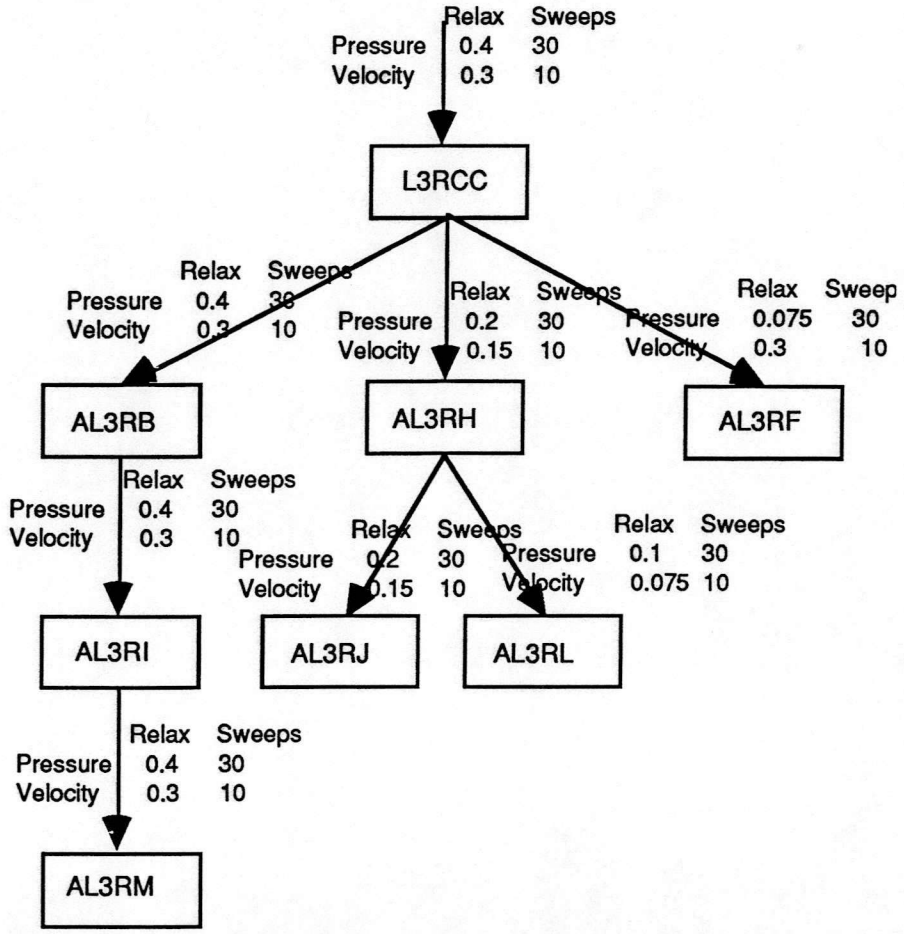

Figure 12 Tree Diagram showing relationships between the relaxation factor optimisation runs

The resultant output from L3RCC was chosen as the initial start variable data set as up to this point the approach shown some potential, only deviating from a converged solution when a change in pressure residual was made. It was therefore decided to continue the run, keeping the same number of sweeps and relaxation factors. These runs were called AL3RB and AL3RI. A drift of inlet pressures, similar to those shown in Figure 10, were seen. The similarity also extended to the final pressures recorded which were of the order -6 kPa. It was concluded at this point that the large numbers of pressure sweeps were not the cause of the experienced instabilities.

The four remaining runs, shown in Figure 12, were further relaxation factor investigations. Runs AL3RH and AL3RJ were completed in parallel with AL3RB and AL3RI, together demonstrating that halving both the pressure and velocity relaxation factors made no difference to the solution apart from slowing down convergence. Indeed an examination of recorded pressure histories showed that both solutions oscillated with the same amplitude and mean, but differed only in frequency (where we draw an analogy between time and the number of solver iterations). As the solver dynamics remain unchanged, we may also deduce that there was no change in stability. The only effect was to lengthen computer run times. This phenomena was demonstrated again by runs AL3RL and AL3RJ , in which the relaxation factors of the former were halved. This confirms that there is, in general, no benefit in reducing both relaxation parameters by the same factor.

Runs AL3RF and AL3RB differed only in pressure relaxation factor. The much smaller value used in AL3RF seemed to remove the high frequency fluctuations in the pressure history plots (compare Figure 13 and Figure 14) without over damping the solver.

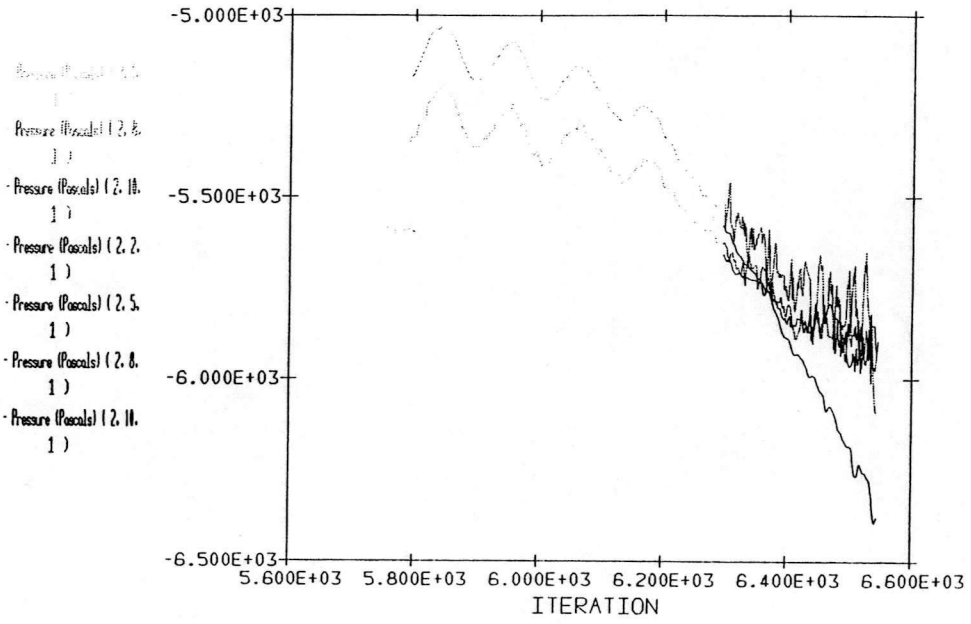

Figure 13 Variation of pressure at inlet: Runs AL3RB and AL3RI

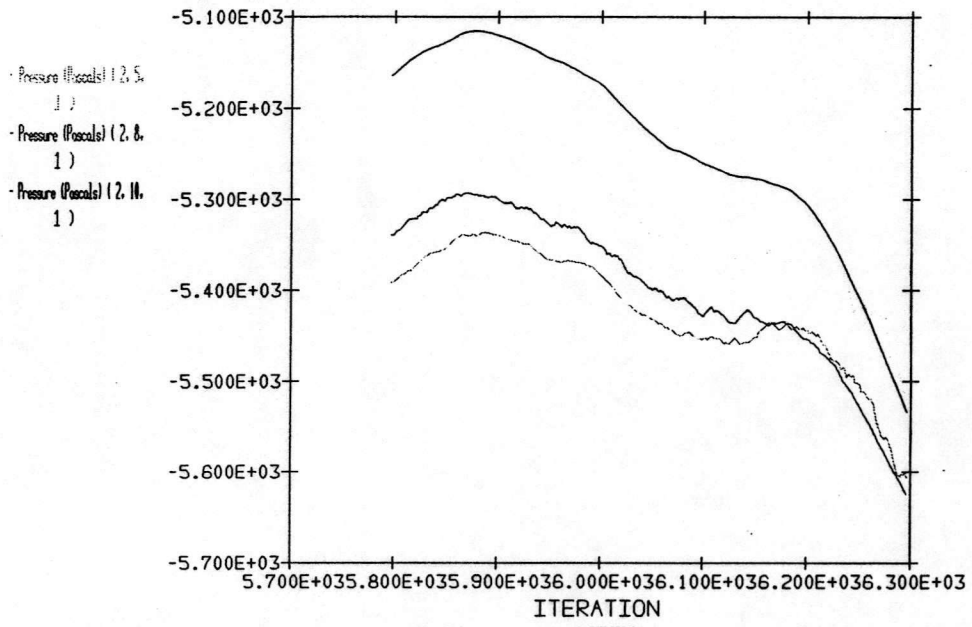

Figure 14 Variation of Pressure at inlet: Run AL3RF

2.2.2.e Reducing the inlet flow rate to help convergence

Runs L3RBBB, L3RDDD and L3REEE were attempts at trying to solve the system of equations at a different fan duty. Instead of an inlet flow velocity of 43 ms^{-1} a value of 35ms^{-1} was used. All of these runs were initially very promising; exhibiting stable characteristics. However, in all of the runs the inlet pressure values diverged before becoming constant. This may be see in Figure 15 .This characteristic behaviour was repeated even when there were corresponding reductions in pressure residual

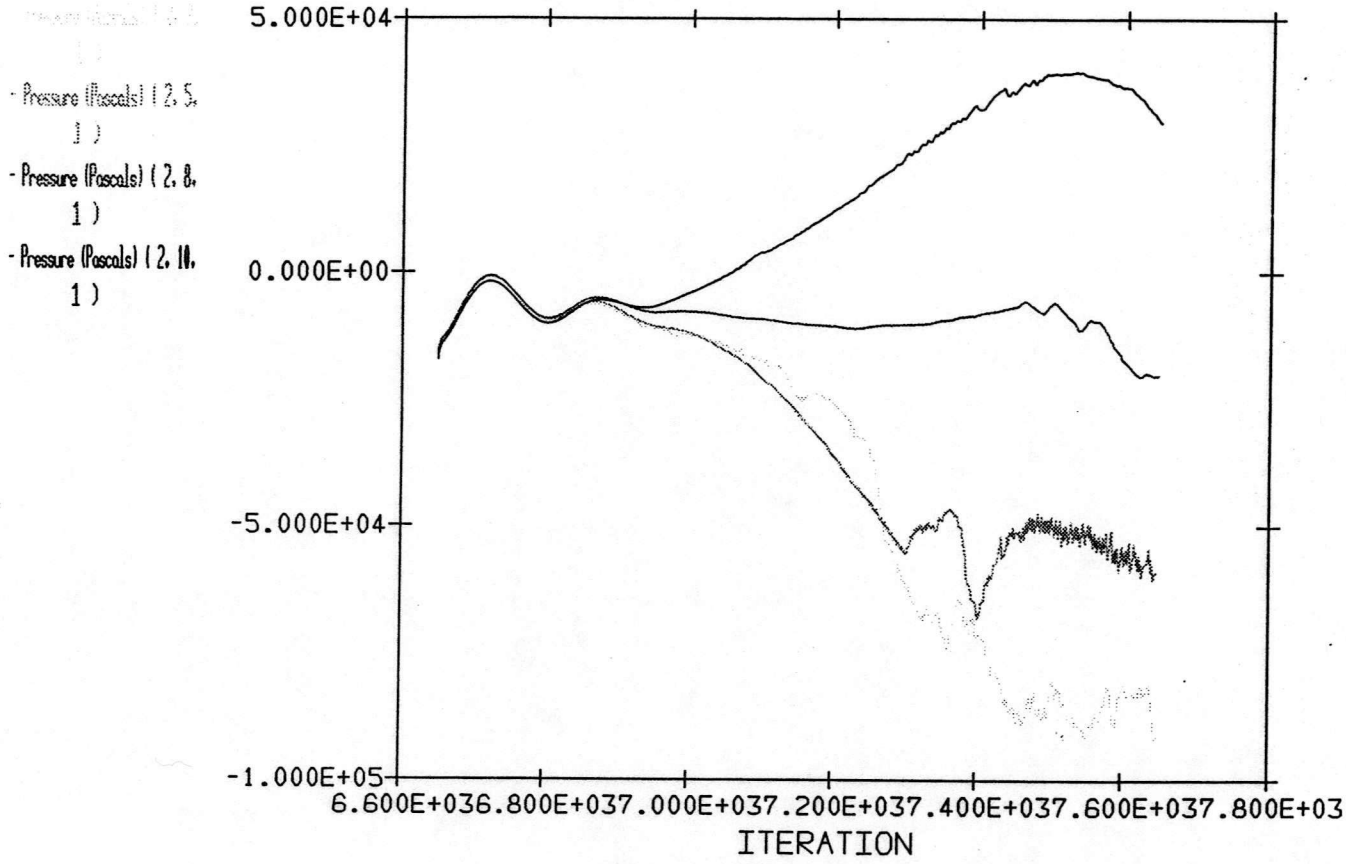

Figure 15 Run L3RBBB: An example of a divergent solution

2.2.3 Single Passage Bladeless Model Runs

The results of the bladeless model computer runs of the simplified L3R impeller are reported and analysed here.

FLUENT allows the user some control over the solution algorithm with options that include changing the iterative 'relaxation' factors and adjusting the number of computational 'sweeps'. However, even after optimising these parameters the solver became unstable when attempting to model at impeller design conditions. To overcome this it was decided to solve the equations using a series of steps in impeller rotational speeds (this was not tried on the first model due to the expected large computational effort needed for the densely meshed domain). At first the fan rotational speed was set a 10% of the experimental value. Once a stable solution was found, the speed was increased by a small increment and the process repeated until the full test speed of 1118 rpm was attained. Each preceding solution acted as the iterative starting point for the next step with the steps in rotational speeds only applied after the user was convinced that the equations had fully converged. In this way the iterative solver did not encounter any of the large iterative changes in variables found when starting from the initial guessed field and attempted to solve the problem in one large step. In physical terms this approach was equivalent to moving the fan operating point gently up a system resistance line. Rotational speeds of 10%, 30%, 50%,75% and of course 100% of the impeller actual test speed were used.

2.2.3.a No Rotation

Having already encountered stability problems with the preceding L3R bladed model, it was decided that some preliminary investigations into stability should be completed. In particular, the authors were interested to see how the solver acted in the absence of the unstablising effect of pressure gradients and swirl. Consequently this model was run without rotation and the residuals noted for future reference. As the problem had neither the swirl or the pressure gradients found in turbomachines, it was relatively easy to solve with no convergence problems encountered. The recorded residuals were used for reference in further runs to help define convergence. Instead of the null inlet flow corresponding to zero rotation, a flow rate representing 10% of design was prescribed. The model yielded a stable solution with the following error residuals after only 500 iterations.

Table 4 Residual values for runs with no rotation

Model Names	Pressure Residual	U-Velocity Residual	V-Velocity Residual	W-Velocity Residual
NAB9-NAB11	$3x10^{-3}$	$1x10^{-2}$	$3x10^{-3}$	$7x10^{-4}$

2.2.3.b Steps towards a full speed solution of the impeller flow at design conditions

The inlet volume flow rate and the body forces corresponding to 10% rotation were applied to the model. With a small number of computational cells, the program could run interactively at reasonable speeds. A numerically stable solution strategy was quickly found. Instead of blindly running the model for a large number of iterations, a series of batch runs were completed with the results regularly examined for signs of convergence. Six batch runs were required before the problem was deemed converged for the 10% flow rate. Corresponding filenames for these runs, and the others that follow, are all prefixed with NAB.

Similar batch runs, as above, were completed with further increases in rotation speed. Again, for every few thousand iterations, the program output was examined. Interestingly all of the computer runs showed similar error residual and variable history characteristics, apart from a small increase in pressure residual. Examination of Table 5 shows the recorded residual values and how they responded to steps in speed.

Table 5 Final Residuals of different speed runs

% Design Flow	Pressure Residual	U-Velocity Residual	V-Velocity Residual	W-Velocity Residual	Number of Iterations
10%	$0.8x10^{-2}$	$5x10^{-4}$	$1.5x10^{-3}$	$5x10^{-4}$	6400
30%	$2.0x10^{-2}$	$4x10^{-4}$	$1.3x10^{-3}$	$5x10^{-4}$	3200
50%	$3.3x10^{-2}$	$4x10^{-4}$	$1.4x10^{-3}$	$5x10^{-4}$	3300
75%	$5.0x10^{-2}$	$4x10^{-4}$	$1.3x10^{-3}$	$5x10^{-4}$	4000
100%	$6.3x10^{-2}$	$4x10^{-4}$	$1.0x10^{-3}$	$4x10^{-4}$	4000

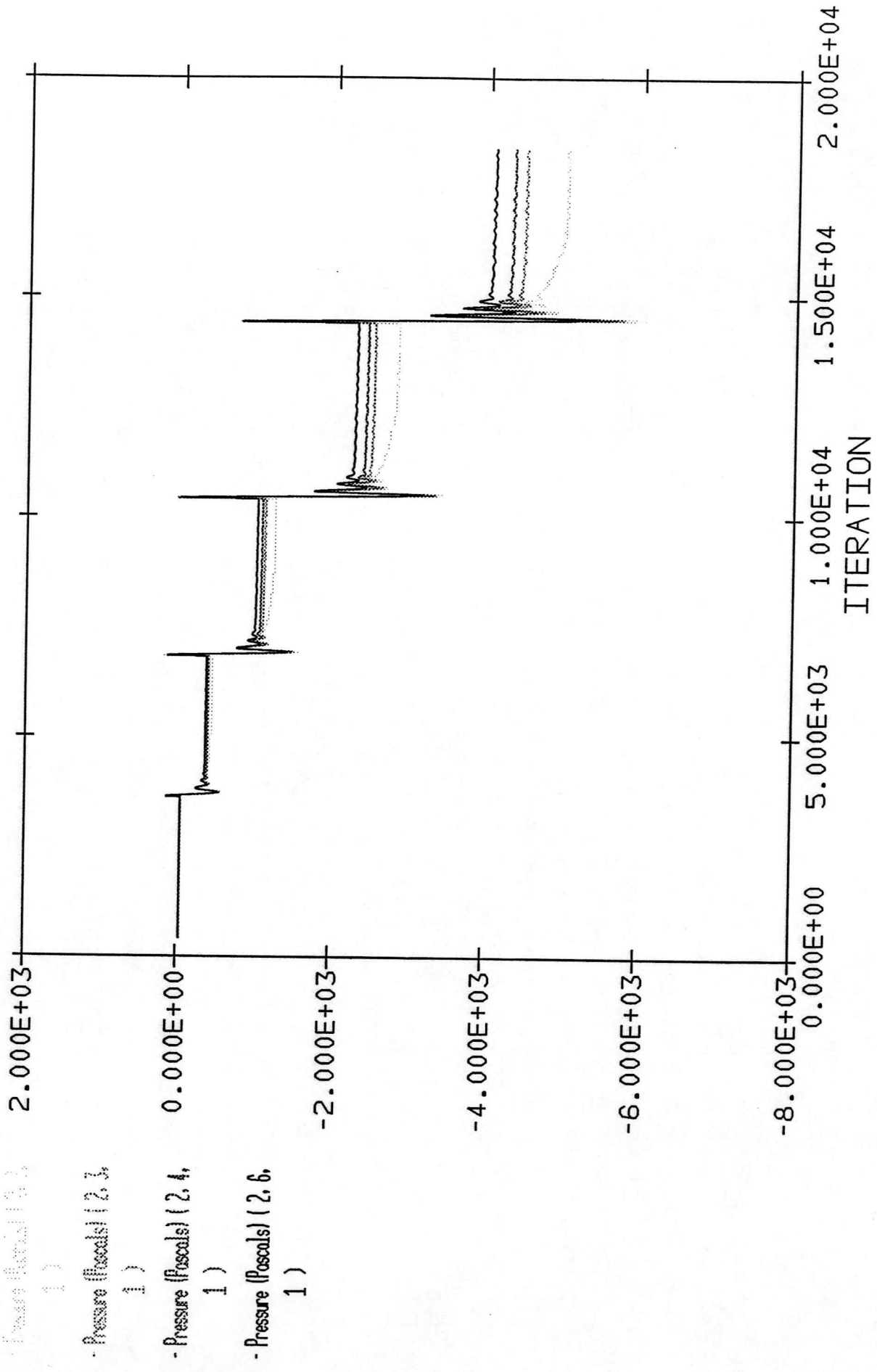

Figure 15 Variation of inlet pressure with steps in fan speed

Likewise the recorded pressures at the inlet duct shown in Figure 15 demonstrate how the solver seemed unaffected by the fan rotational speed. Together with the experience gained from the previous L3R 'bladed' and the PHOENICS Mizuki investigations, we may conclude that the solution parameters may need tuning for modelling different fan system resistances, but are best kept constant for changes in speed.

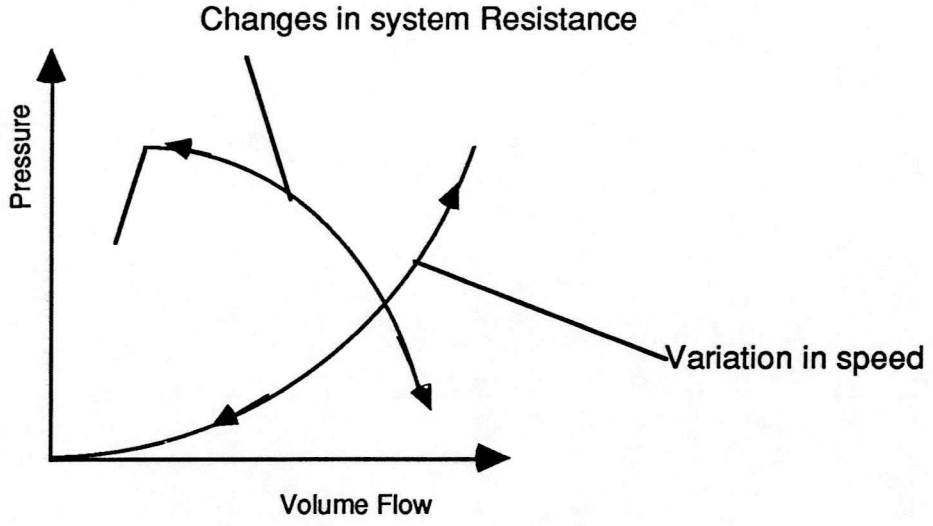

Figure 16 Changes in duty either by speed or system resistance

2.2.3.c Prediction of fan performance

The choice of boundary conditions used in the CFD model corresponded to the L3R fan test completed by Bennett and Watson[1991]. See Figure 22 below.

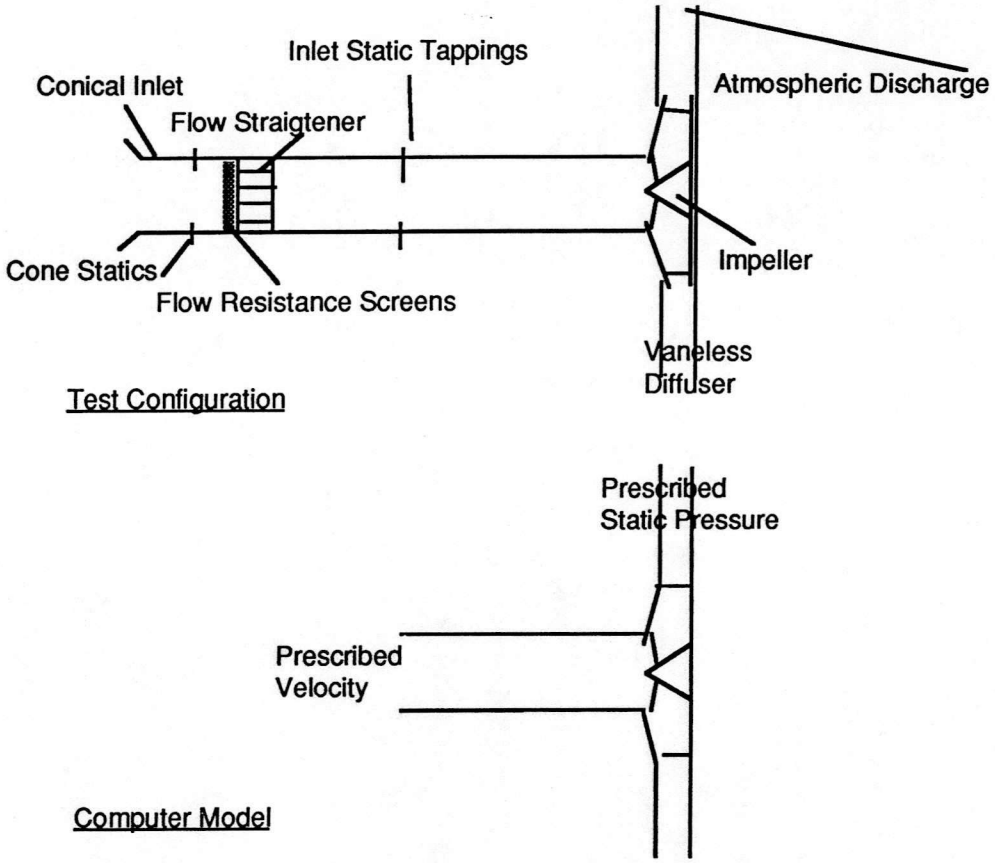

Figure 18 Comparison of Fan test and CFD model boundaries.

In addition to calculating the velocity field, the CFD model was able to predict a fan pressure rise. This involved using the inlet pressure field and is explained below.

2.2.3.d Fan Pressure Rise Definitions

Firstly we must define what is meant here by the term 'fan pressure rise' .
The following definitions are inherent within BS848:Part 1:1980

Fan Total Pressure, $P_{tF} = P_{t2} - P_{t1}$

$= P_{v2} - P_{t1}$ (as the discharge gauge static pressure is zero)

Fan Static Pressure, $P_{SF} = P_{tF} - P_{v2}$

$= P_{v2} - P_{t1} - P_{v2}$

$= -P_{t1}$

where $()_2$ denotes the conditions at impeller discharge

$()_1$ denotes the conditions at impeller inlet

$()_v$ denotes velocity head

Therefore to specify the fan static pressure only requires the measurement of the fan total pressure, $-P_{t1}$ at inlet. For the CFD model this required some special averaging as the prescribed inlet pressure was far from uniform.

2.2.3.e Calculation of fan inlet total pressure

The inlet total pressure consists of an earth-frame-relative velocity head and a static pressure. The inlet velocity head was calculated from the prescribed axial inlet velocity and density. Due to the inlet pressure field asymmetry an averaging technique was necessary to calculate a corresponding inlet static pressure. For this the 5 x 5 inlet computational mesh values were mass flow weighted.

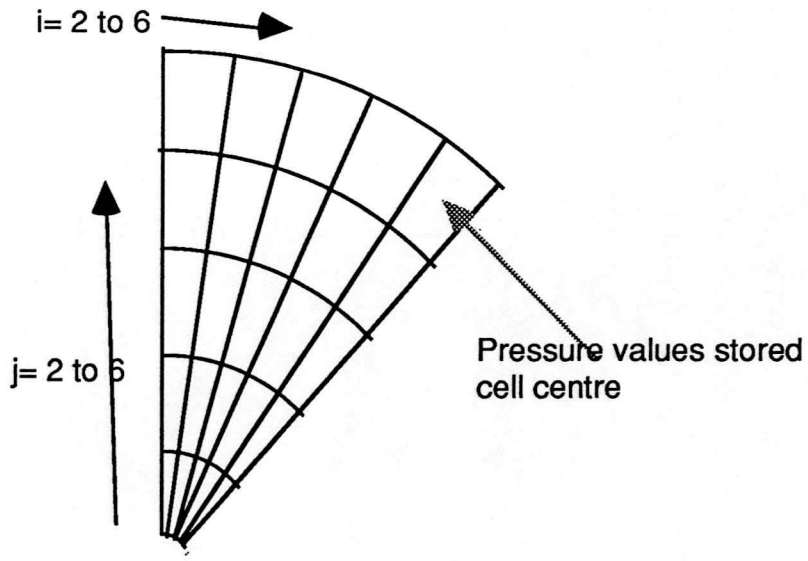

Figure 19 Inlet finite volume cell structure

The inlet pressure was calculated using the following expression

$$p = \sum_{j=2}^{6} w_j \sum_{i=2}^{6} \frac{1}{5} p_{i,j}$$

where i and j refer to the cell co-ordinates in Figure 19
and the weighting w_j is given by

$$w_j = \frac{r_j^2 - r_{j-1}^2}{r_6^2}$$

where r_j is the outer radius of cells with ordinate j.

i.e.

Table 6 Weighting Applied

radius (m)	j	weighting, w_j
0.592	6	0.36
0.4736	5	0.28
0.3552	4	0.20
0.1184	3	0.12
0	2	0.04
	total =	1.00

This weighting technique was applied to the computer solutions calculated earlier. The results are given in Table 7 below.

Table 7 Predicted Fan Static Pressure Rise

% of Actual impeller test speed	Mass Weighted inlet static pressure (Pa)	Prescribed axial inlet velocity (ms^{-1})	Calculated Fan Static Pressure P_{sF}' (Pa)	Experimental Fan Static Pressure P_{sF} (Pa)	Ratio of experimental to CFD predicted pressures P_{sF}/P_{sF}'
10 %	-42.3	2.104	39.6	24	0.606
30 %	-381	6.267	357	212	0.594
50 %	-1060	10.441	995	589	0.591
75 %	-2380	15.664	2233	1325	0.593
100 %	-4230	20.886	3968	2356	0.594

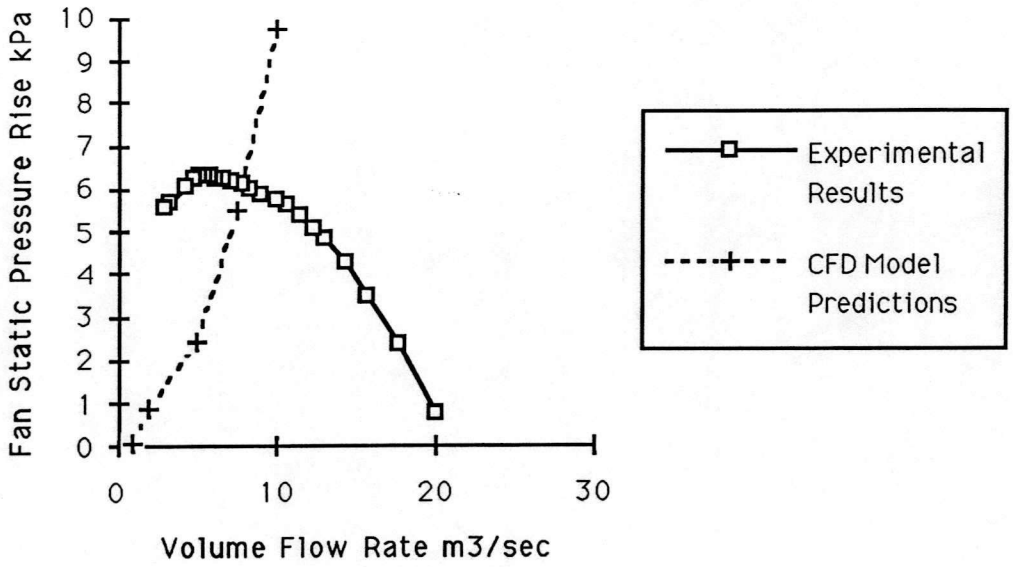

Figure 20 Path of CFD model variable speed runs

As can be seen from Table 7 the ratios of calculated fan static pressure rise to those found in experiment are remarkably consistent. This ratio may be thought of as a kind of efficiency, with the computational results representing the ideal performance. With this we can gain further assurance of the computation model accuracy , as in reality the fan speed has very little effect on fan efficiency at low Mach numbers.
It should be re-iterated here that this inviscid model was in no way expected to predict the overall fan performance. Its isothermal, incompressible and inviscid formulation make it unable to predict losses. This is apparent in Figure 20 where the results from the CFD model are plotted with the actual aerodynamic test results. The point of maximum pressure predicted by the CFD model should coincide with the equivalent experimental pressure at the same volume flow rate. It is expected that proper modelling of flow turbulence would reduce the discrepancy.

2.2.3.f Steady State Pressure/Volume Excursions

The inlet flow rate was varied to model different operating points on the fan characteristic. Conditions representing Peak Efficiency, High flow rate, at stall and deep stall were all modelled. The predicted fan static pressures rises, analysed as in the previous section, did not follow or even shadow the fan characteristic curve. Indeed the fan static pressure rise predicted was almost constant. These runs are tabulated below, starting with the high volume flow rate case.

*Table 8 Fan Static Pressure Rise Predictions referred to 1m conditions**

Computer Run	Flow Condition	1m Flow Rate (m^3/sec)	Predicted Fan Static Pressure Rise (kPa)	Experimental Fan Static Pressure Rise (kPa)
PV51	High	13	9.1	4.8
NAB61	Design	10	9.8	5.8
PV2	Peak Efficiency	7	9.9	6.2
PV4	Stalled Flow	4	9.9	5.8
PV11	Highly Stalled Flow	2	10.0	5.0

*1910 rpm, 1m diameter impeller, density = 1kg/m^3

The most apparent phenomena seen in the predicted velocity fields is the inception and subsequent growth of large recirculating regions at flow rates corresponding to stall. These can be seen in the velocity vector plots of Figures 21 to 25.
The nature of these stall cells is not yet fully understood but we can deduce that they were not generated by viscous forces, as the flow model was completely inviscid; or by some thermal energy transfer, as the model equations were isothermal.

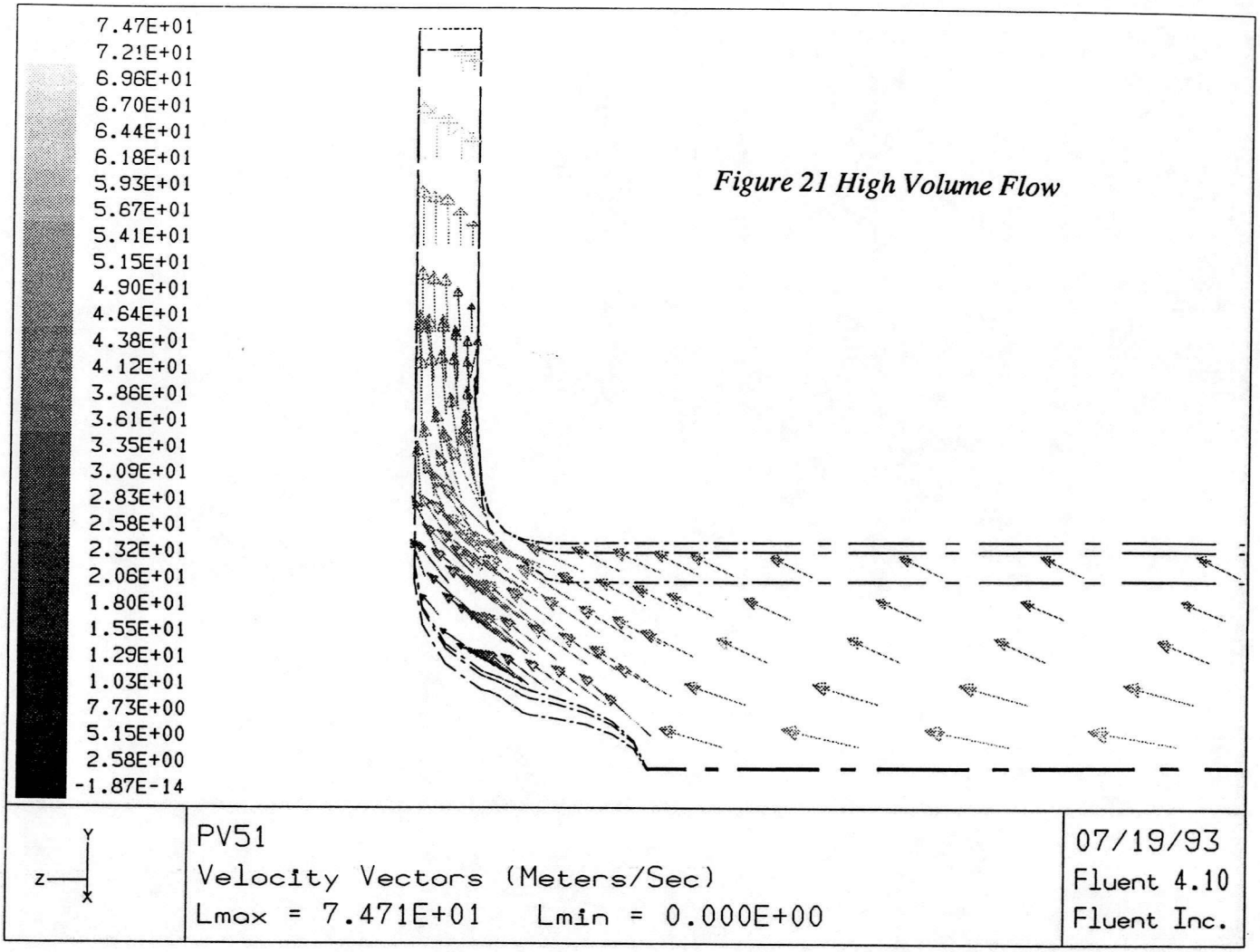

Figure 21 High Volume Flow

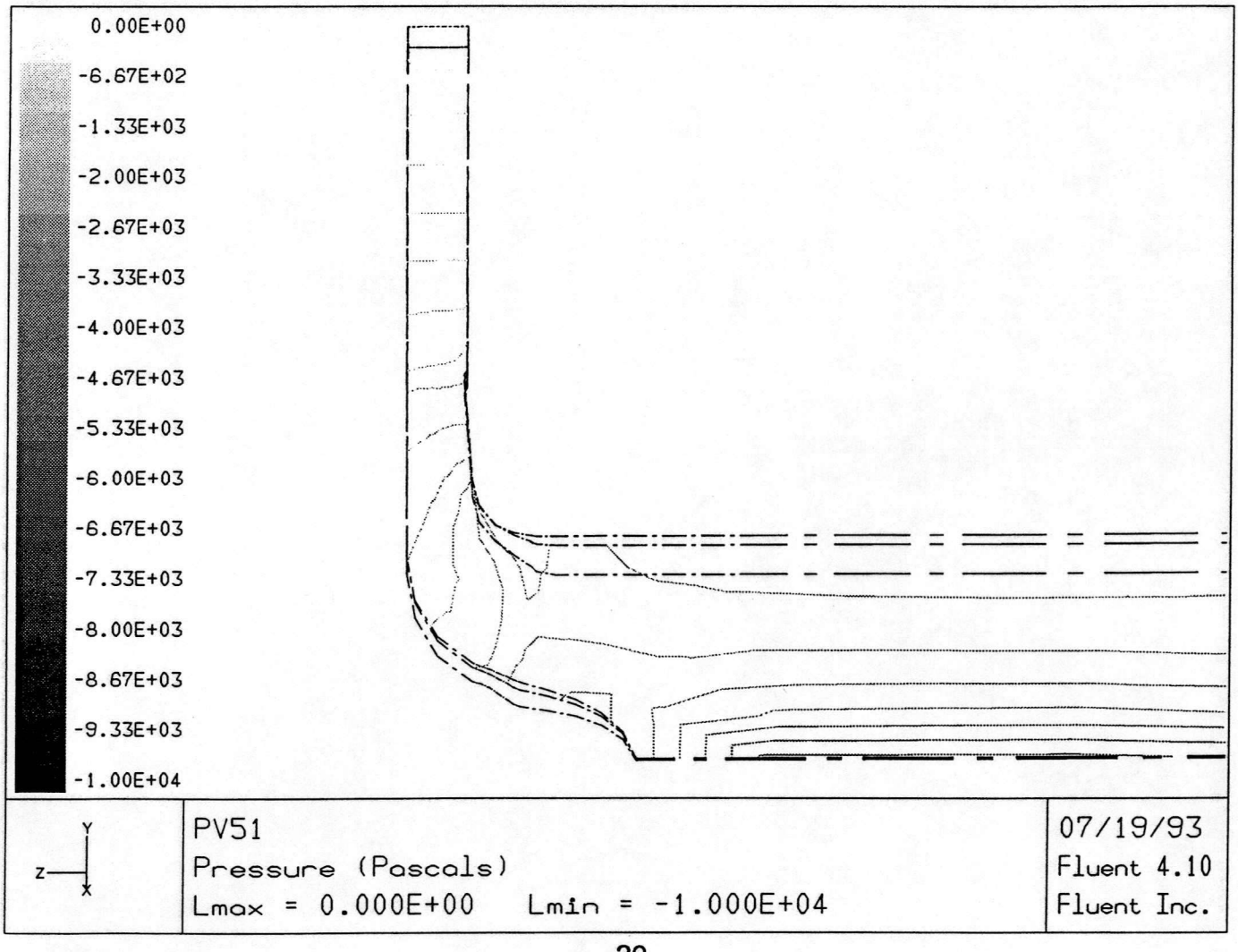

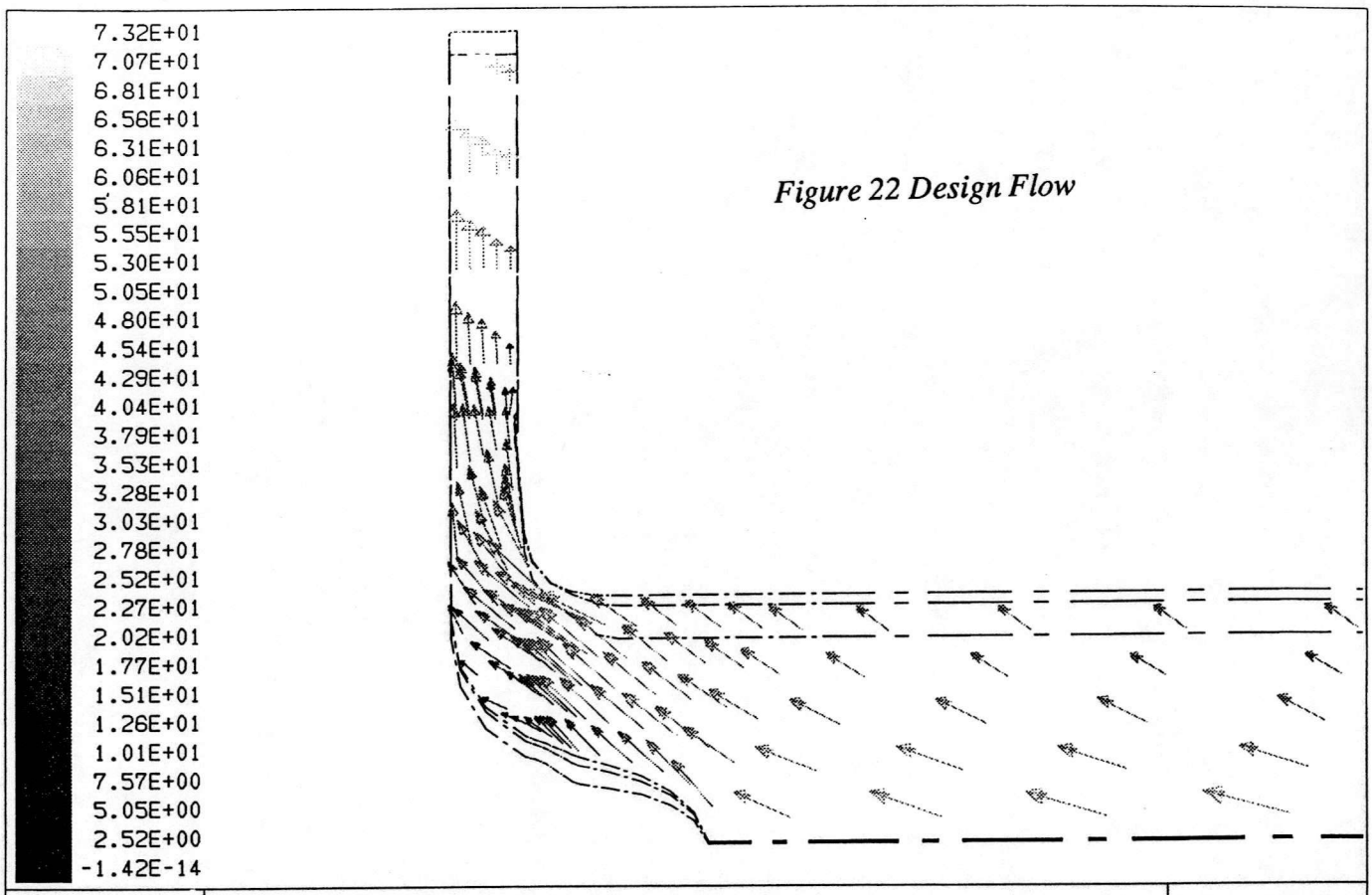

Figure 22 Design Flow

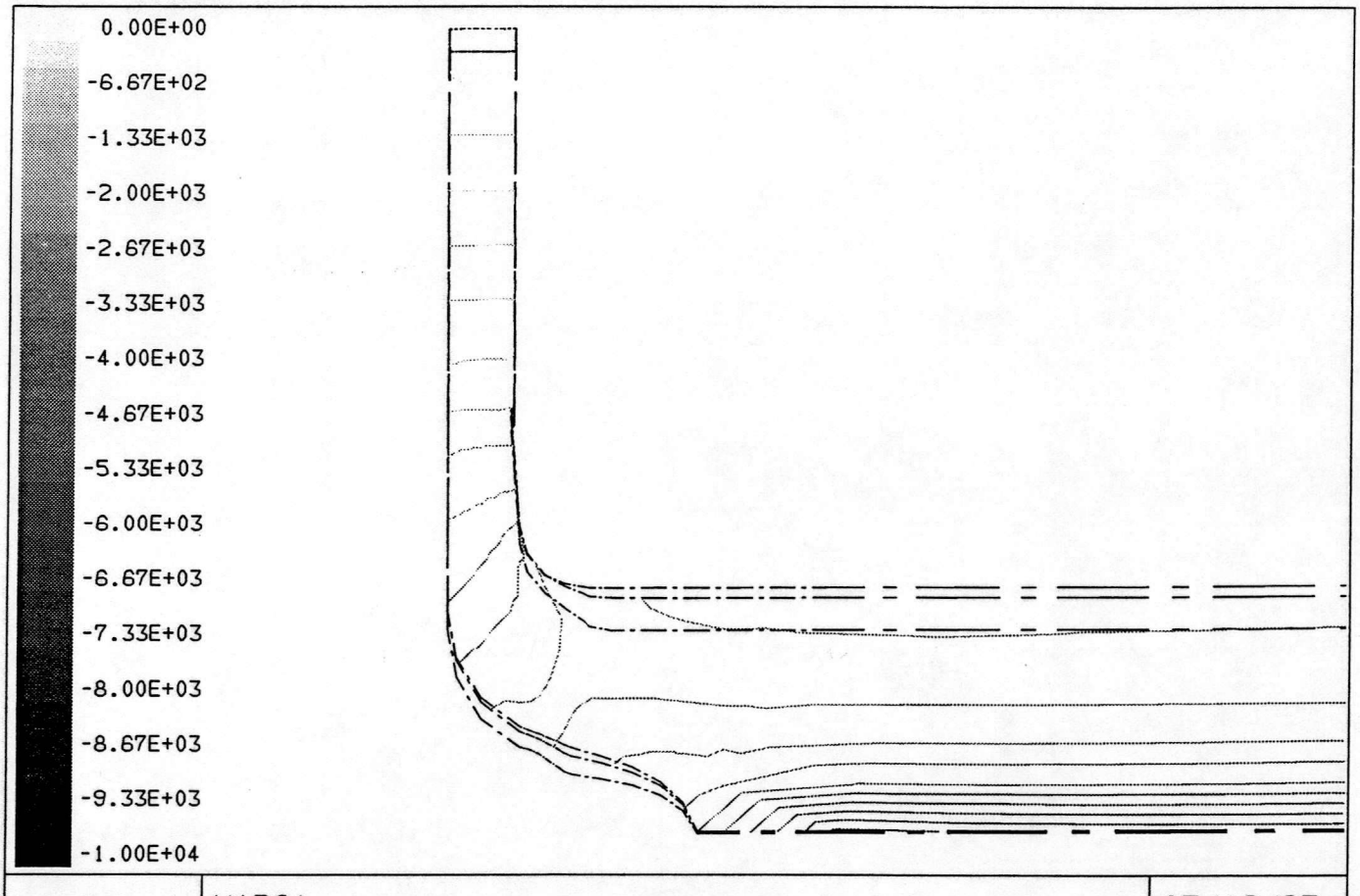

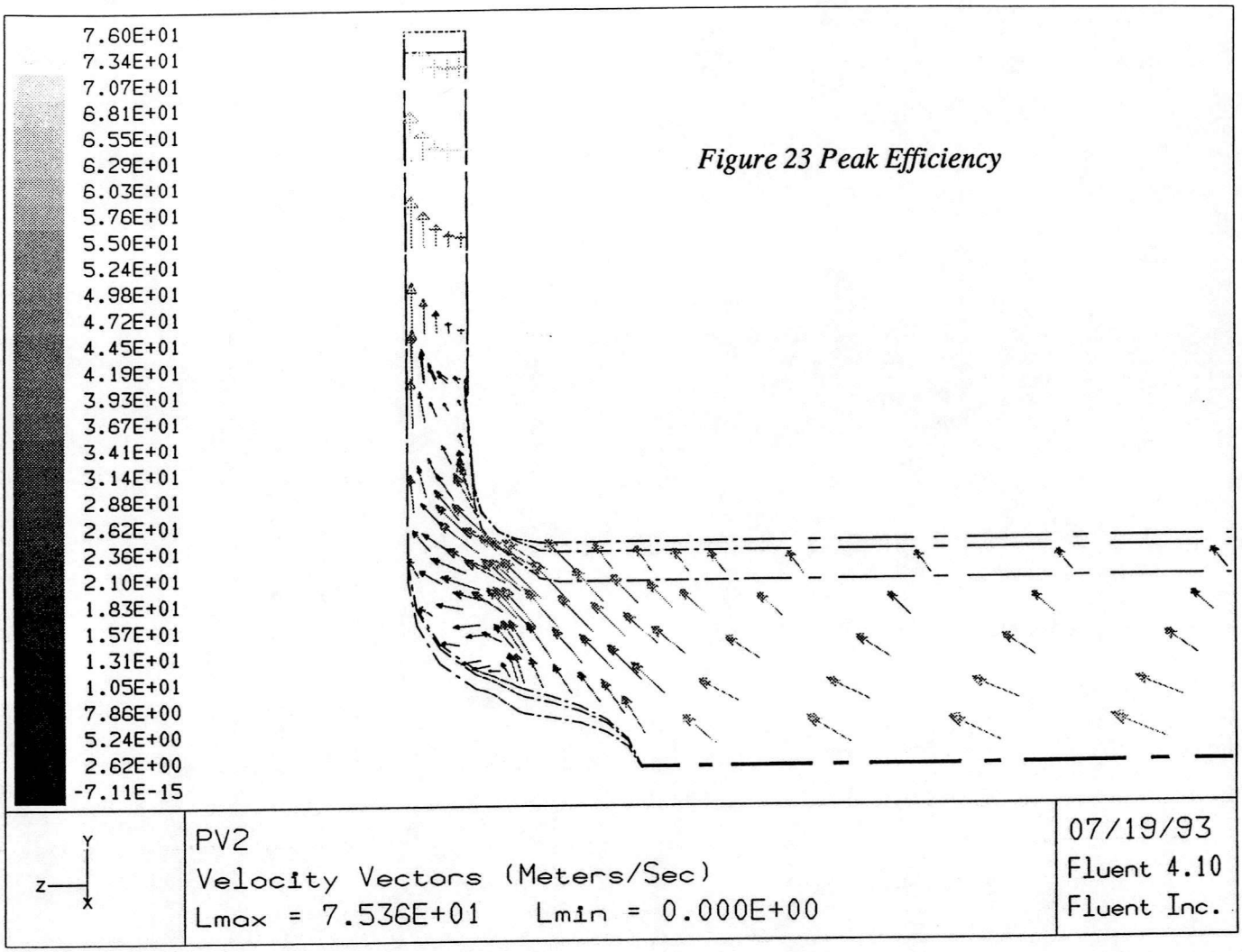

Figure 23 Peak Efficiency

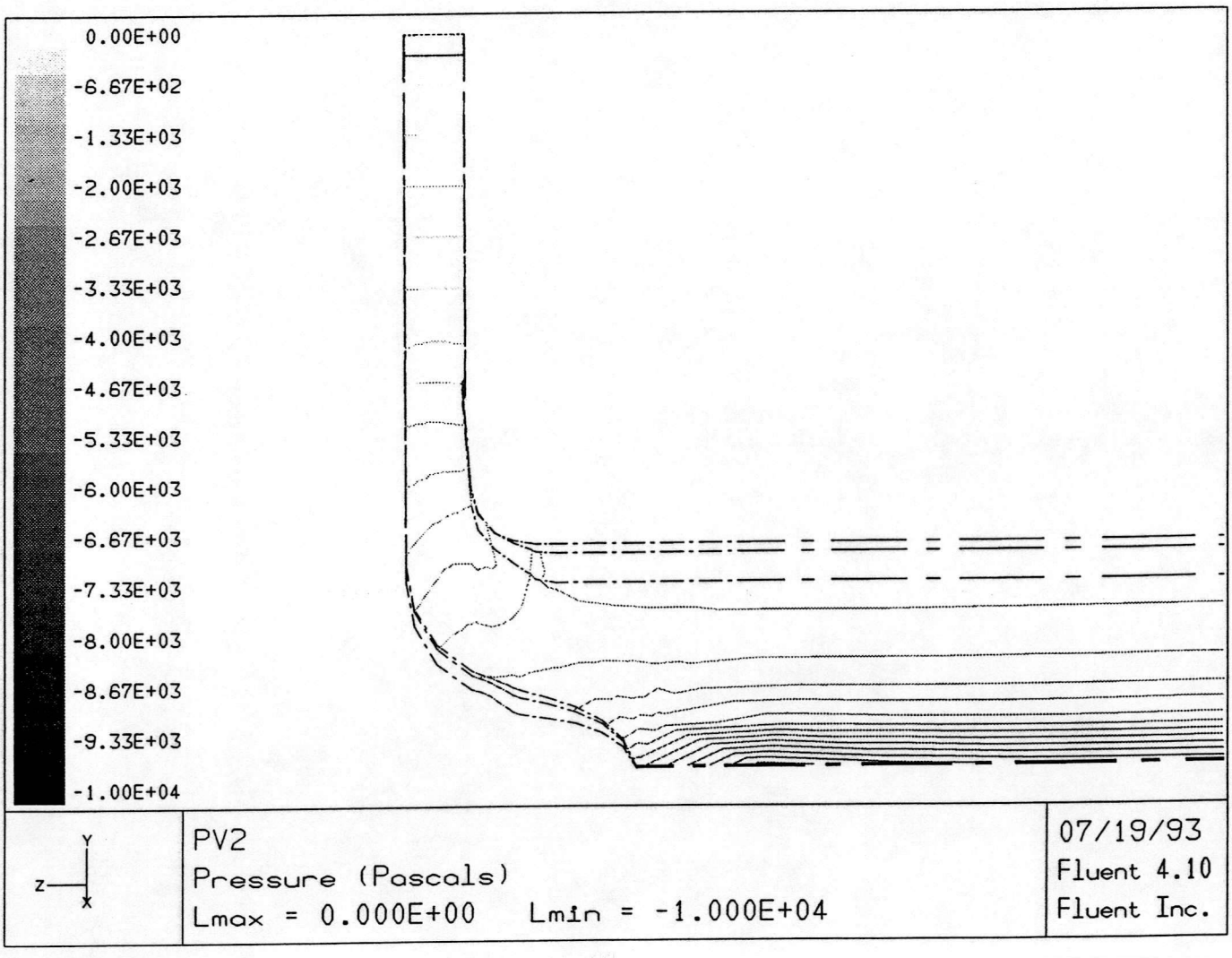

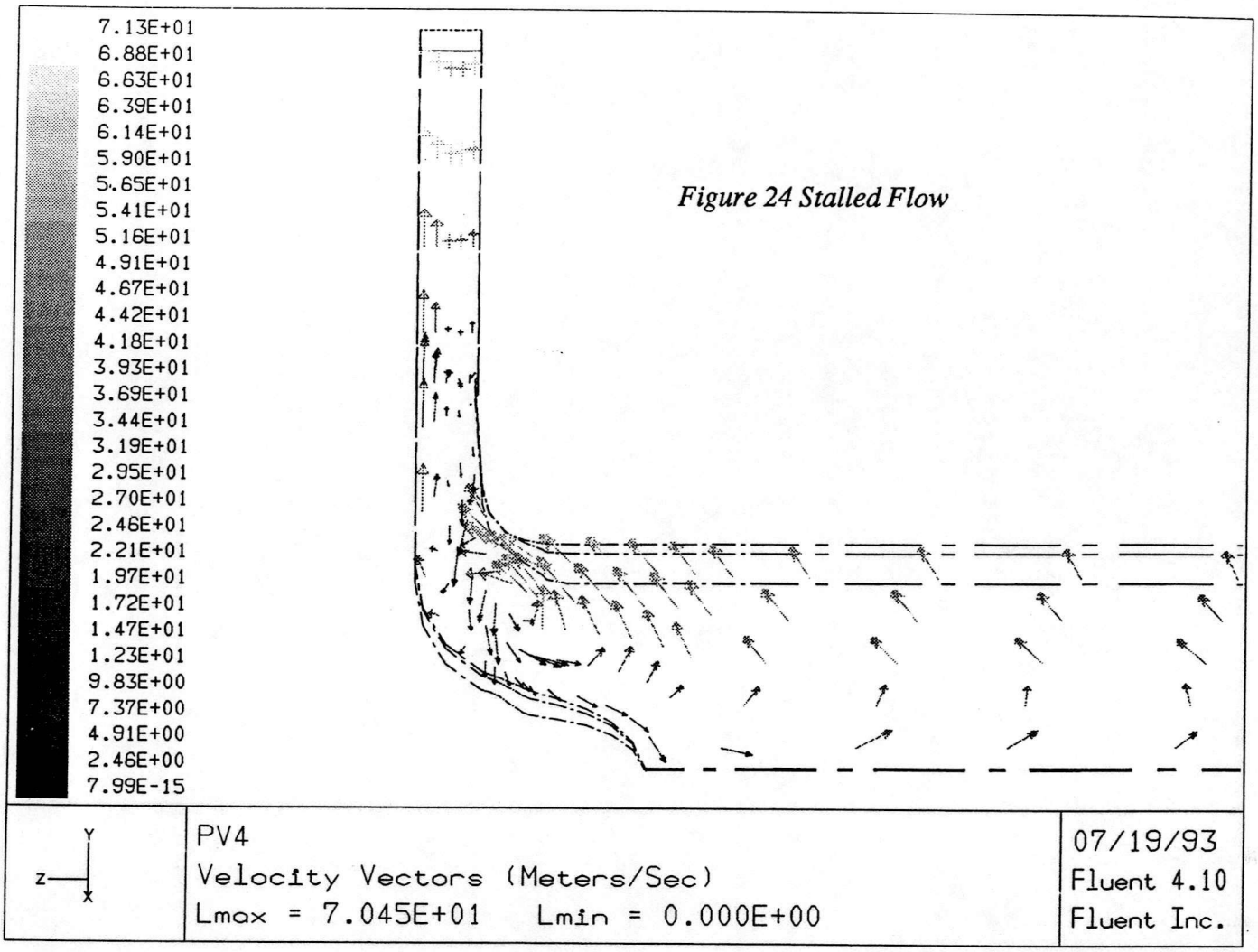

Figure 24 Stalled Flow

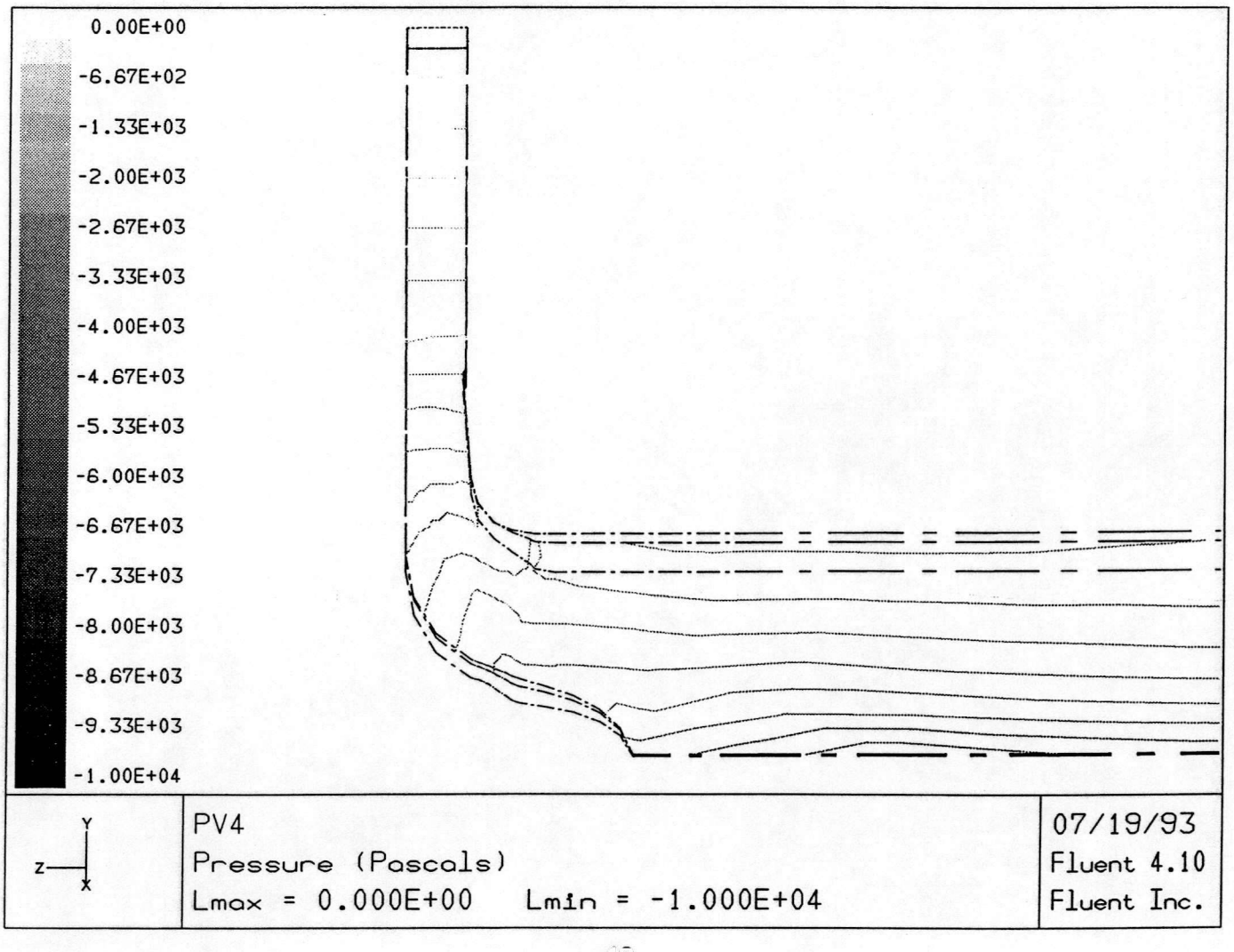

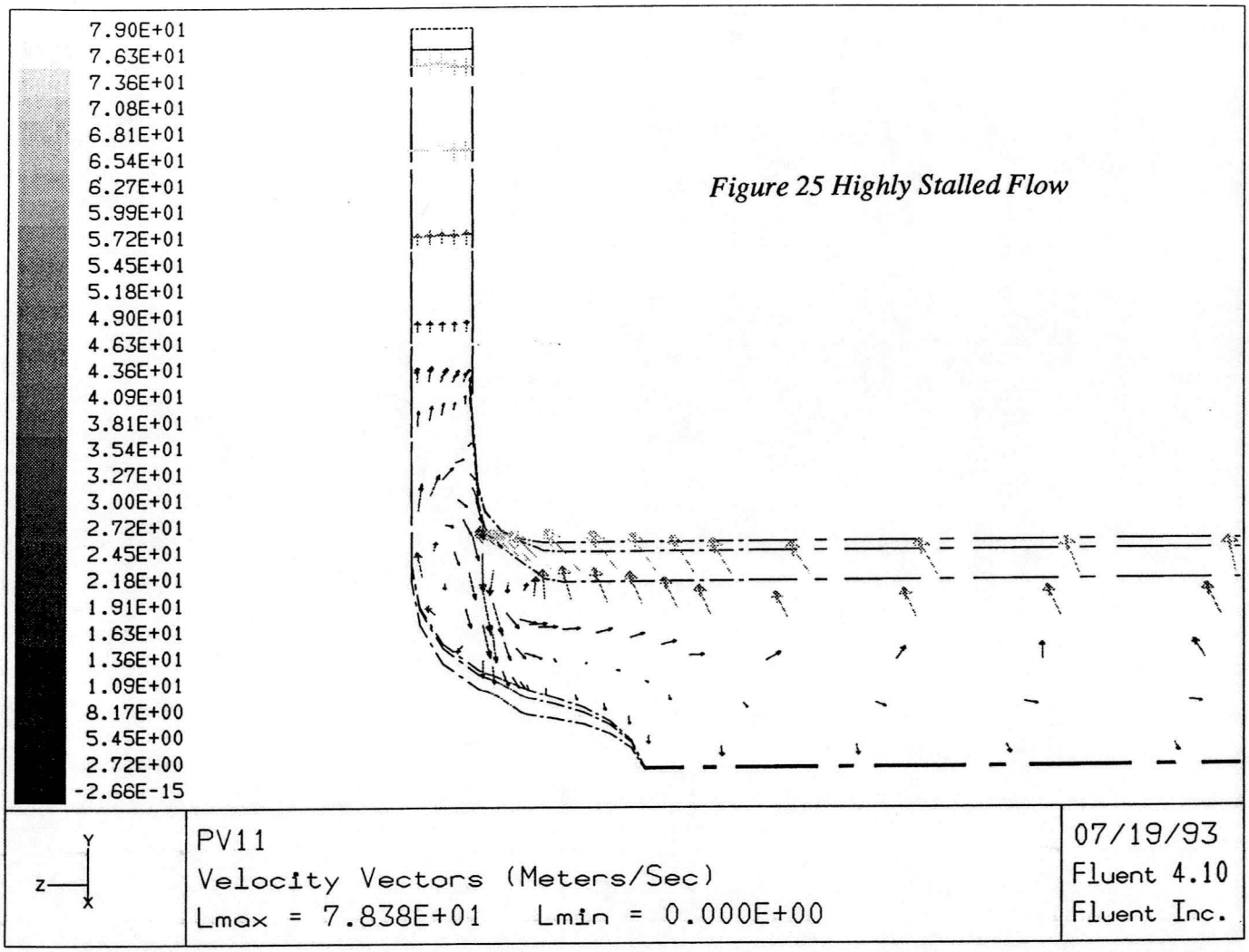

Figure 25 Highly Stalled Flow

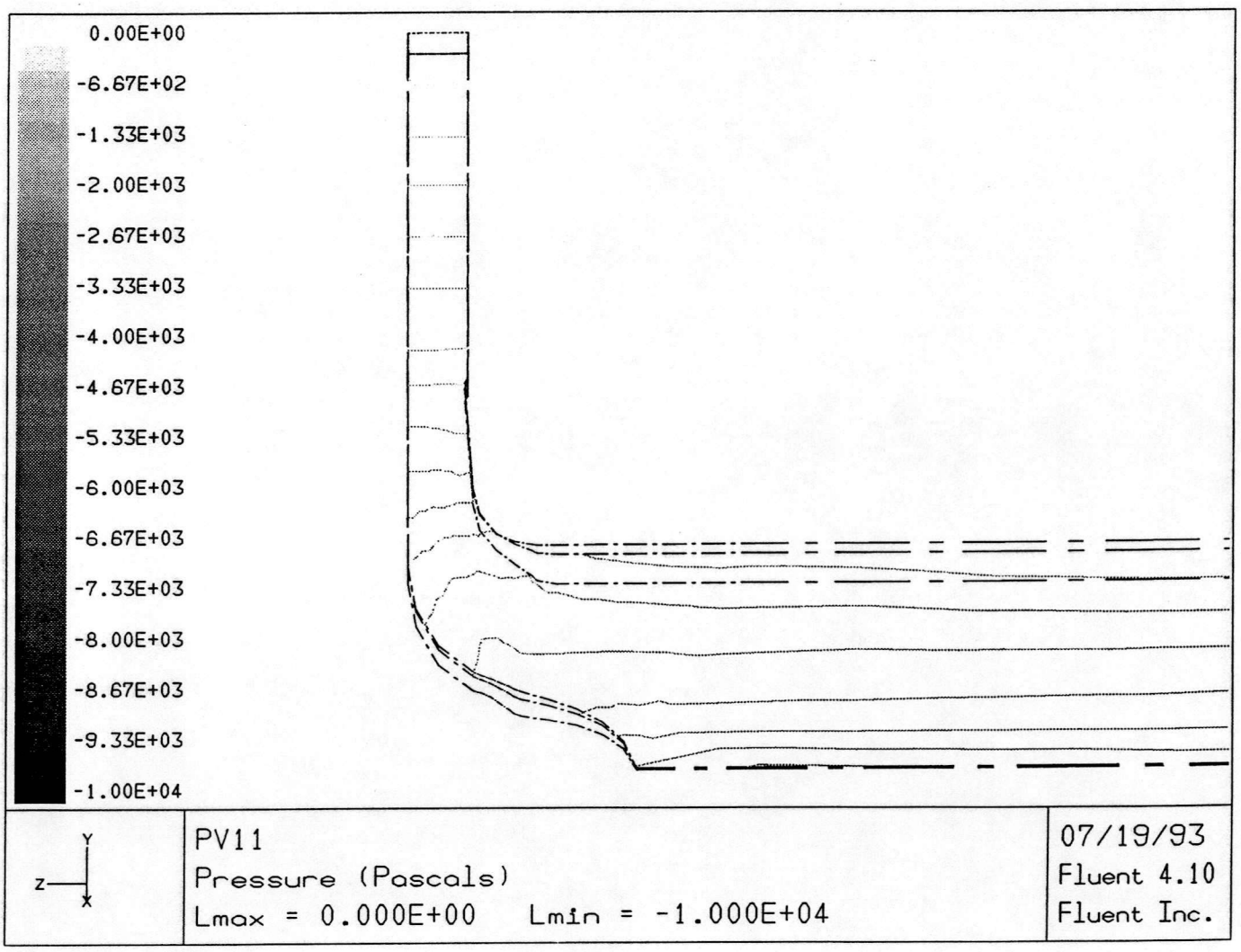

2.2.3.g Numerical Convergence

The residual for the above runs are tabulated below, together with the number of iterations completed at each stage. For all cases the number of computational sweeps and the relaxation parameters were unchanged.

Table 8 Pressure/Volume Excursion Runs: Error Residuals

Run Name	Description of Flow	Number of iterations	Pressure Residual	U-Velocity Residual	V-Velocity Residual	W-Velocity Residual
PV51	High	3000	1.2×10^{-1}	1.2×10^{-3}	2.6×10^{-3}	7.7×10^{-4}
NAB61	Design	4000	6.3×10^{-2}	4.2×10^{-4}	1.0×10^{-3}	3.8×10^{-4}
PV2	Peak Efficiency	3000	5.4×10^{-2}	4.6×10^{-4}	1.4×10^{-3}	4.1×10^{-4}
PV4	Stalled Flow	2000	2.1×10^{-1}	1.6×10^{-3}	5.5×10^{-3}	3.7×10^{-3}
PV11	Highly Stalled	2000	1.3×10^{-1}	8.1×10^{-4}	5.1×10^{-3}	2.2×10^{-3}

There is a noticeable trend of increased residual as we move away from the fan design conditions. This was noticed as well in the PHOENICS Mizuki impeller investigation.

Figures 26 to 30 show how the inlet pressure field varied during the iterative cycles for each of the flow rates. We can use the design flow variable history diagram as a reference.

The flows above are described starting from the highest flow rate, i.e. PV51. For case PV51 the field variables demonstrated some oscillatory (with respect to iteration) motion. The amplitude of pressure oscillations at the inlet was approximately 100 Pa. As can be seen in Table 8, this motion did not effect the overall error residuals. Next, using the design flow solution, NAB61, as the initial start data set, the flow at peak efficiency was predicted. The inlet pressure field showed stability, apart from the innermost cells which represented the inlet duct central core. There, some random motion was seen. However the mass-weighted contribution of these small cells is negligible and this was consequently of little concern. In the run corresponding to stalled flow, PV4, similar disturbances were apparent outside the central core, stretching right across the complete inlet plane. On further flow reductions, these perturbations remained.

Figure 26 High Volume Flow
-Inlet Pressure Variation

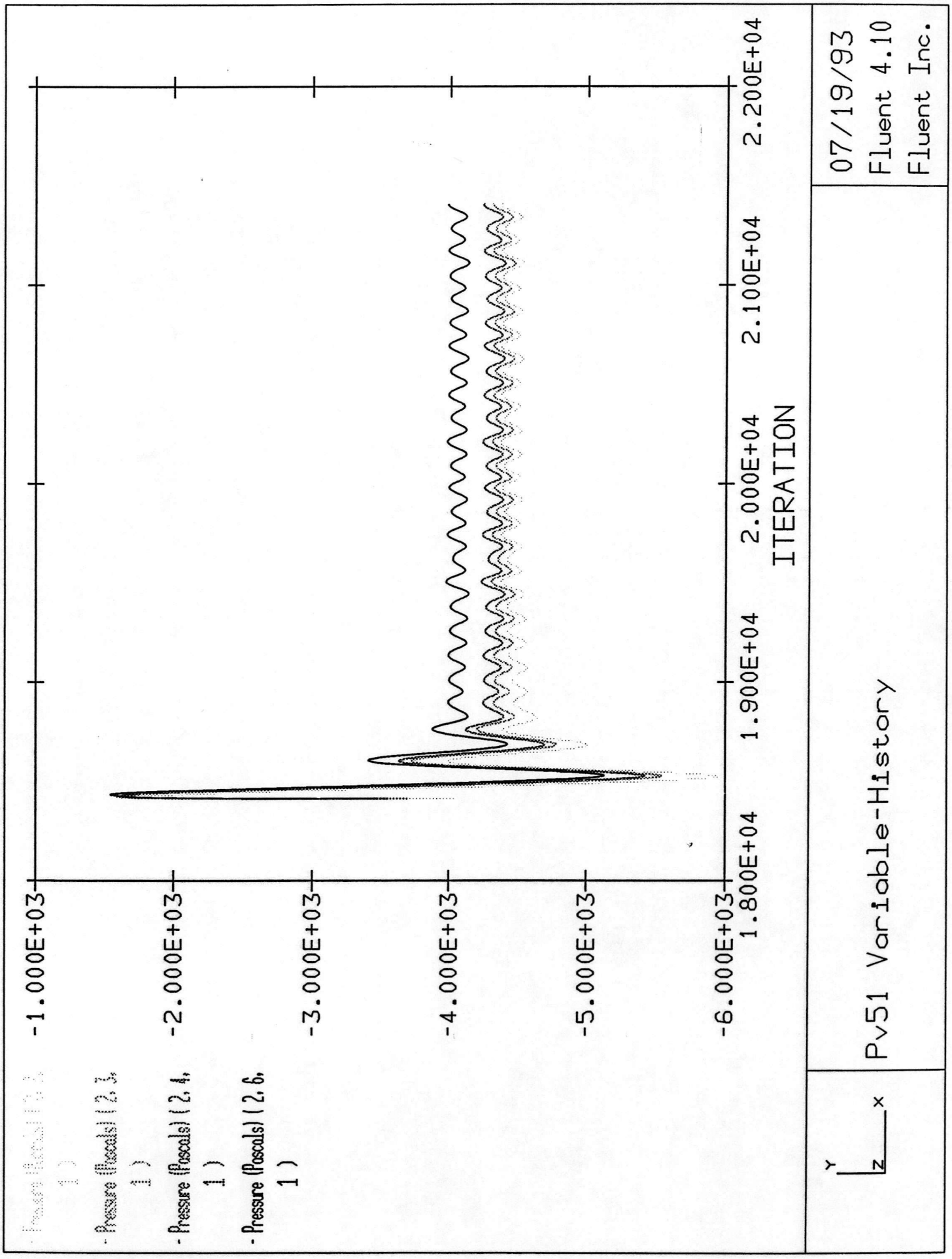

Figure 27 Design Flow
-Inlet Pressure Variation

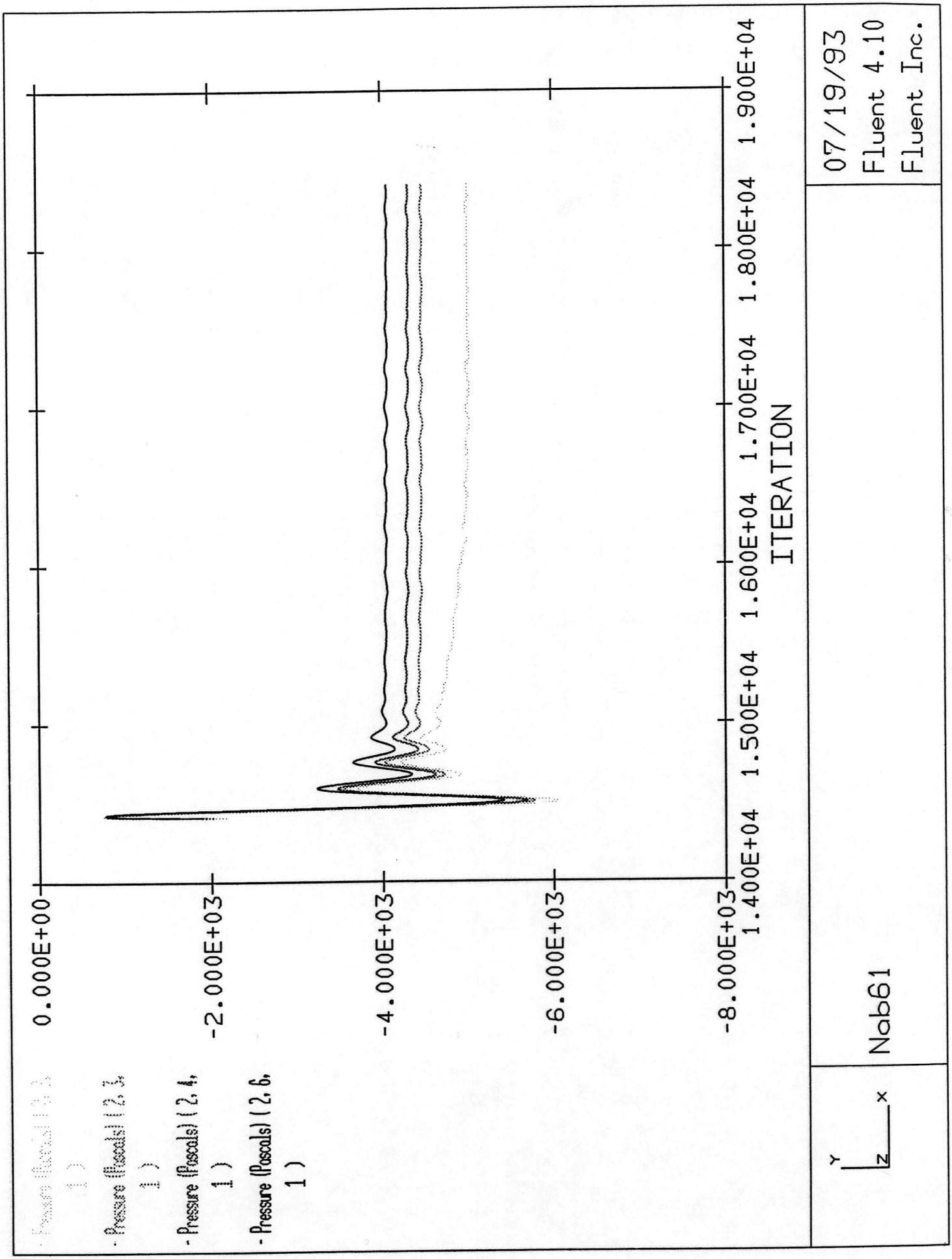

Figure 28 Peak Efficiency
-Inlet Pressure Variation

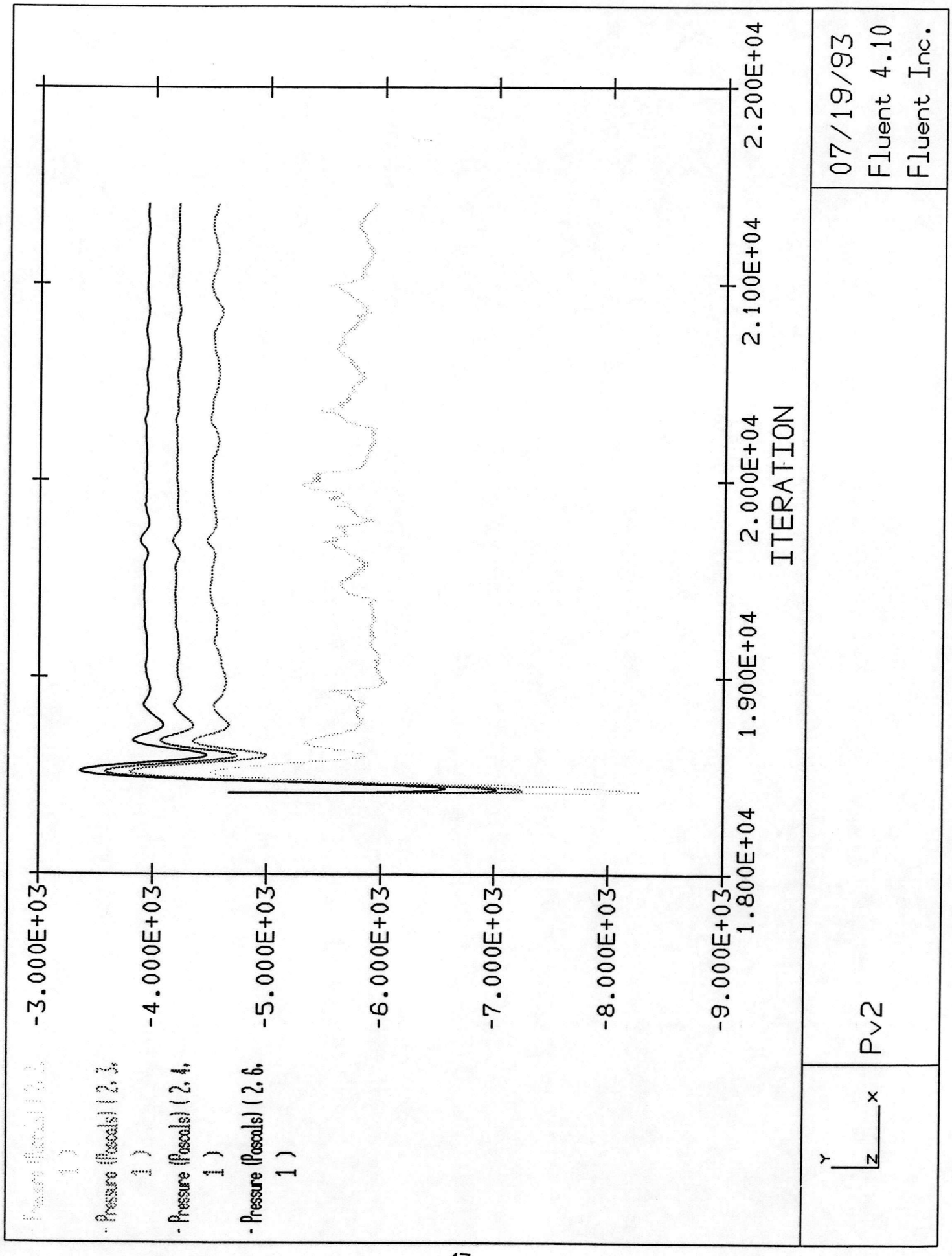

Figure 29 Stalled Flow

-Inlet Pressure Variation

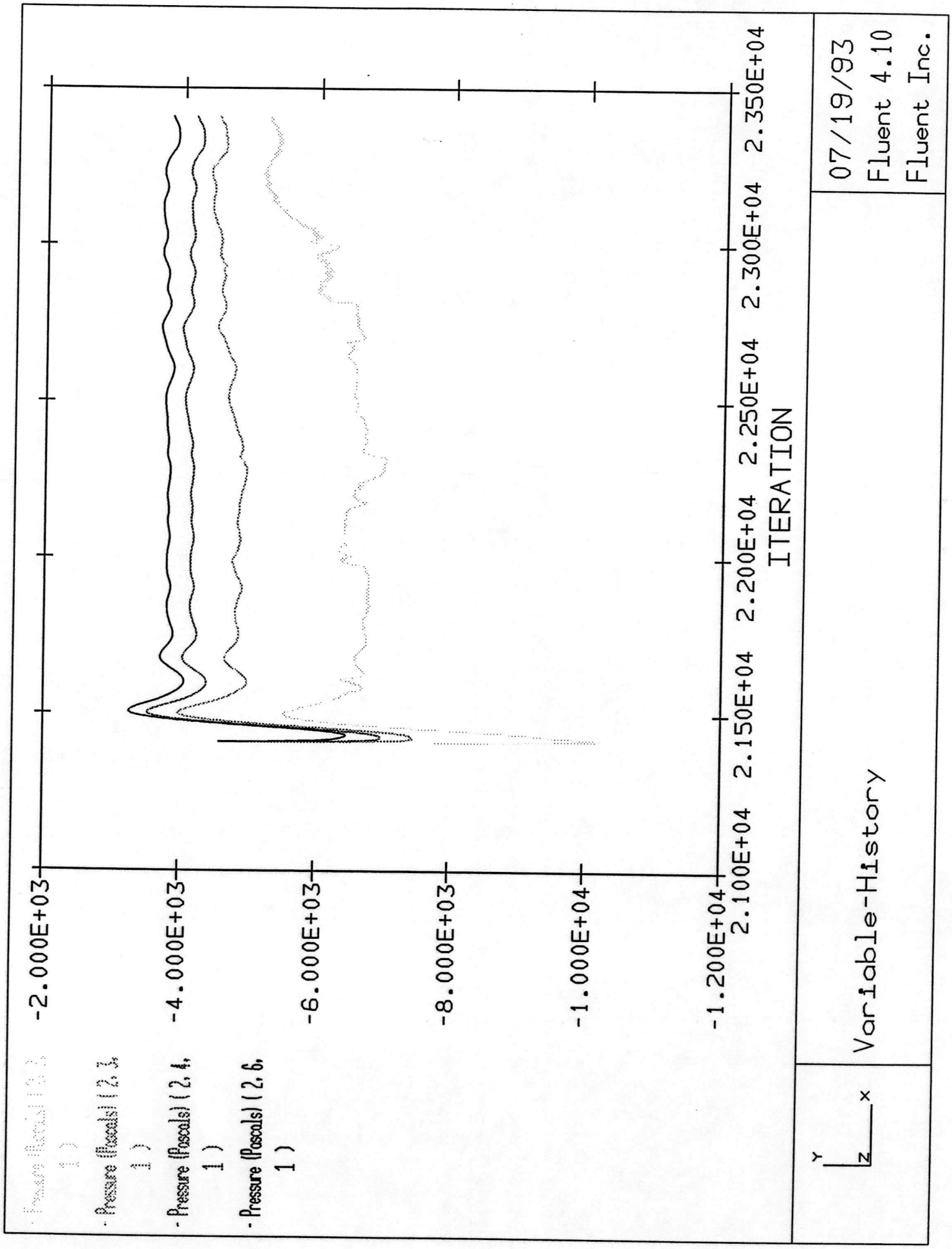

Figure 30 Highly Stalled Flow
-Inlet Pressure Variation

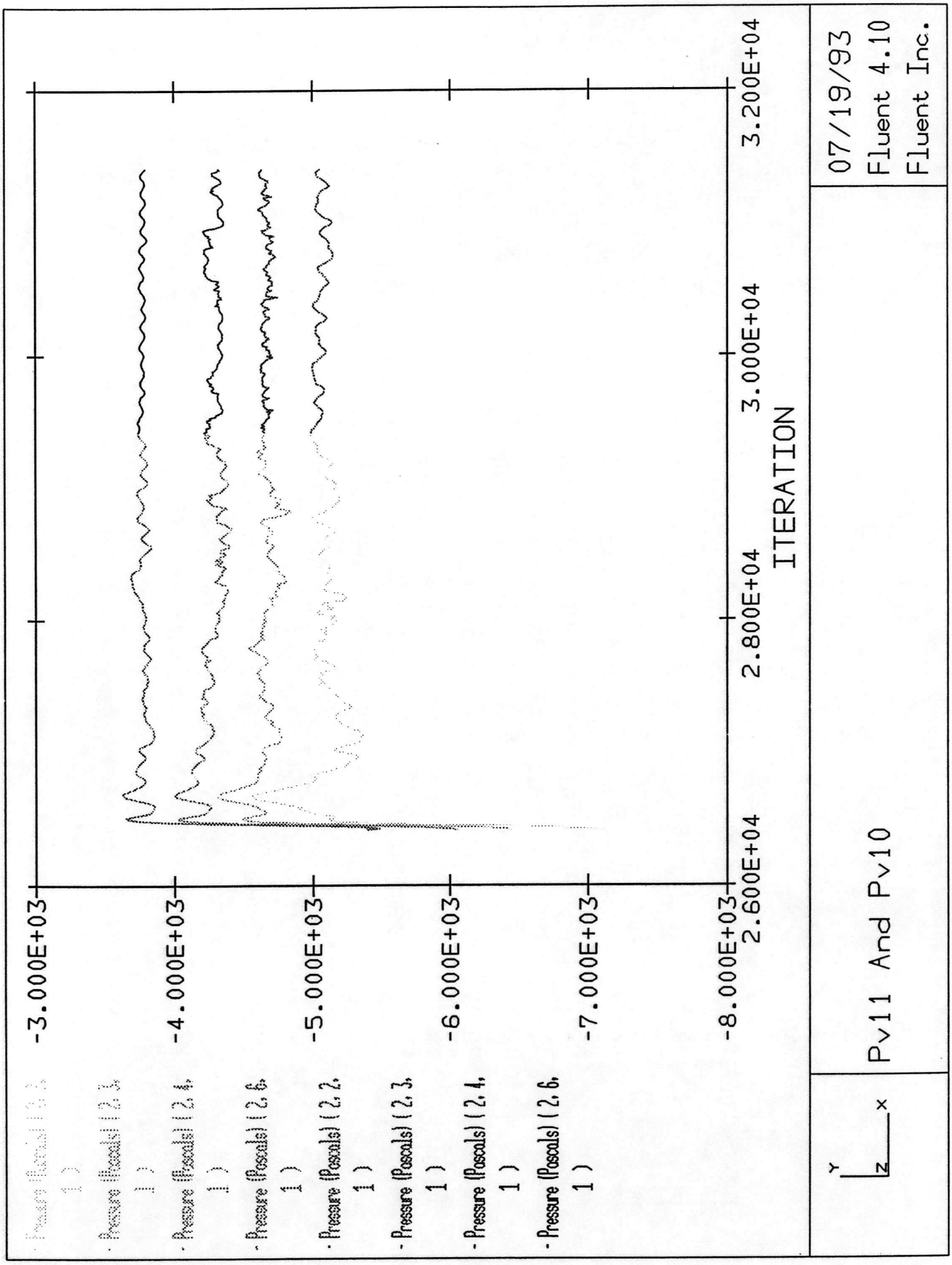

2.2.4 Incompressible Time-Dependent Runs

Having succeeding in gaining converged solutions for a multitude of flow conditions using the bladeless L3R model, it was decided to invoked the time dependent option available in FLUENT. It was hoped to predict unsteady stall cells as demonstrated by Bosman [1984]. The authors, however did had some reservations as Bosman allowed for compressibility in his finite volume time-marched model. Here the flow was set as incompressible. As per the rest of this report, all runs are tabulated for easy reference.

Table 9 Incompressible Time Dependent Model Runs

Run	Flow Condition	Pressure Residual	U-Velocity Residual	V-Velocity Residual	W-Velocity Residual	Time Step (secs)	Max No. of iterations	No of time steps
NAB72	100%	$6x10^{-2}$	$5x10^{-4}$	$1x10^{-3}$	$5x10^{-4}$	0.05	50	20
NAB73	100%	$7x10^{-2}$	$5x10^{-4}$	$1x10^{-3}$	$5x10^{-4}$	0.05	50	40
NAB75	100%	Diverged	Diverged	Diverged	Diverged	0.005	50	N/A
NAB77	100%	Diverged	Diverged	Diverged	Diverged	0.005	100	N/A
NAB114	40%	$1x10^{-1}$	$1x10^{-3}$	$2x10^{-3}$	$1x10^{-3}$	0.2	100	20
NAB214	20%	$1x10^{-2}$	$7x10^{-4}$	$5x10^{-3}$	$1x10^{-3}$	0.5	100	4
NAB219	20%	$9x10^{-2}$	$8x10^{-4}$	$1x10^{-3}$	$4x10^{-3}$	0.04	200	20

All the above models incorporated the following solution parameters

Table 10 Solution Parameters

Variable	Number of Sweeps	Relaxation Factor
All Velocities	3	0.3
Pressure	10	0.1

In addition, some investigations into the stability of the models with respect to time step were completed. To ensure good comparison the data set from NAB219 was used as the start data set.

Table 11 Time step investigations- All runs were UNSTABLE

Time	Number of Sweeps		Relaxation Parameters	
Step	Pressure	Velocity	Pressure	Velocity
$1x10^{-3}$	10	3	0.1	0.3
$1x10^{-4}$	10	3	0.1	0.3
$1x10^{-5}$	10	3	0.1	0.3
$1x10^{-6}$	10	3	0.1	0.3
$1x10^{-7}$	10	3	0.1	0.3
$1x10^{-8}$	10	3	0.1	0.3
$1x10^{-9}$	10	3	0.1	0.3
$1x10^{-4}$	30	3	0.1	0.3
$1x10^{-4}$	50	3	0.1	0.3
$1x10^{-4}$	100	10	0.1	0.3

For time dependent runs, the user is able to change other solution parameters which control the time step, the maximum residual sum for ceasing iterations and the maximum number of iterations per time step. The latter is used by FLUENT to trigger a progression onto the next time interval should the current interval solution not sufficiently converge to the level set by the prescribed maximum error residual sum. Presumably the original idea behind this utility was two-fold. Firstly it would prevent the solver iterating indefinitely should the solver never be able to converge to the level required. And secondly, should the time step solution converge rapidly, it would prevent unnecessary iterations from being completed, as the solver would move on automatically to the next time step.

However, for the L3R unbladed model runs the pressure residual term dominated the residual sum and it was not thought that it alone would be a representative indication of convergence. Therefore the approach taken in the following runs was to set a generous number of 'maximum iterations' that would ensure that the equations had converged over the prescribed time step. Clearly this was somewhat wasteful in computer time, but it did help to stabilise the solver.

2.2.4.a Discussion of model runs

It was decided that the first time dependent model should be of design flow as this operating condition had shown to be the easiest to converge. With the same solution

parameters as in the previous section, twenty time steps of 0.05 secs were calculated and the run was saved as NAB72. Examination of the reported variable history file showed that all of the recorded variables settled apart from some negligible numerical fluctuations. In addition, for these runs, the variable history measuring stations included the blade passage shroud where recirculation was predicted on the earlier stalled flow model runs. Comparison of meridonial velocity distributions showed, as would be expected for the design flow condition, no differences between the time dependent run and the steady state equivalent. To ensure that the model was completely stable, a further 40 time steps were satisfactorily completed and stored under filename NAB73. The time step of 0.05 secs was chosen as this approximately represents the period of one fan wheel rotation and it was thought that this comparably large time step would help yield a stable solution from which to attempt further runs. It would act as a base from which smaller time step runs, that were necessary to pick up the centrifugal fan unstable flow phenomena, could be started.

To detect rotating stall we must be able to track a stall cell as is crosses a blade passage. This movement takes approximately 0.012 seconds for this particular case. Sensible time steps to capture this phenomena are one or two orders of magnitude less. However further reductions in time step from 0.04 seconds yielded formulations with no stability (see Table 11); even in conjunction with changes in the number of sweeps which in previous runs had shown to stabilise.

Attention was then turned to running a reduced flow model. NAB114 was set to operate in stall with only 40 % of the design flow. A time step of 0.04 seconds was used with the final results identical to the equivalent steady state run, PV4. Reduction of the flow rate further to 20% of design pushed the fan model into deep stall. A time step of 0.04 secs was tried for this condition but the equations became unstable and it became necessary to increase this to 0.5 secs before stability was regained. With this large time-step no unsteady flows were detected. A second and successful attempt at using 0.04 seconds for the highly stalled condition was completed using 200 iterations, rather than 100, per time step. Despite the small time step, no fluctuations in the recorded velocities were noted.

A variation in the frequency of the inlet pressure perturbations was noticed when the variable histories of runs NAB114, NAB214 and NAB219 were compared. These may be seen in Figures 31-33.

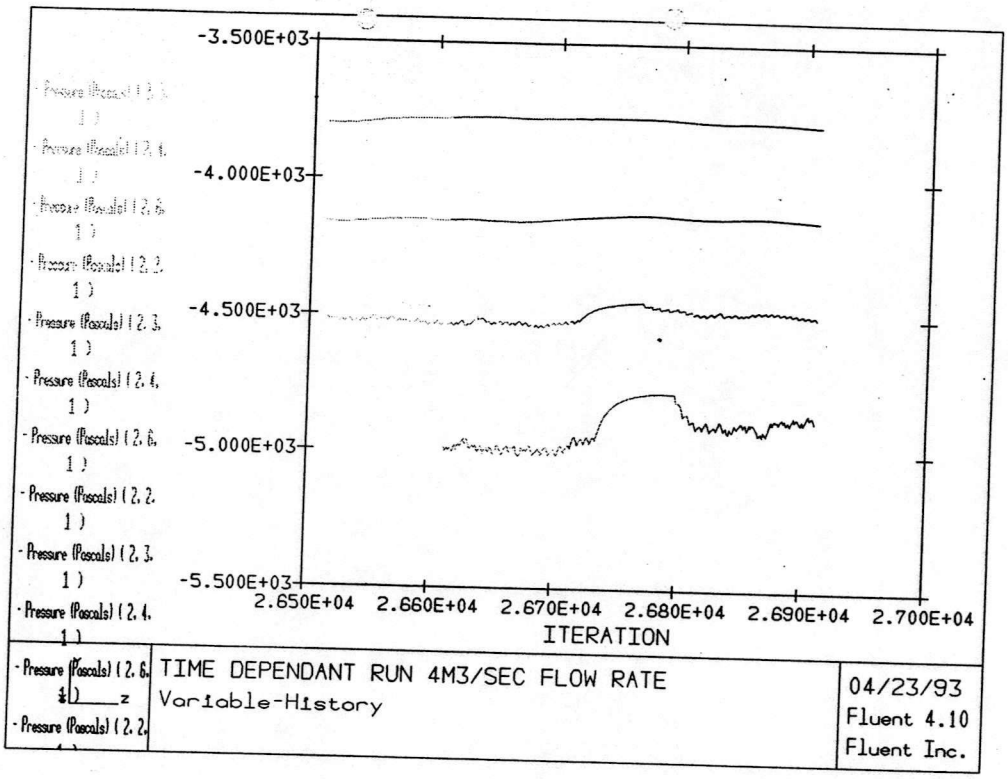

Figure 31 *Inlet Pressure Variable History, NAB114*
(40 % design Flow, Time Step 0.2 secs, 100 iterations per time step)

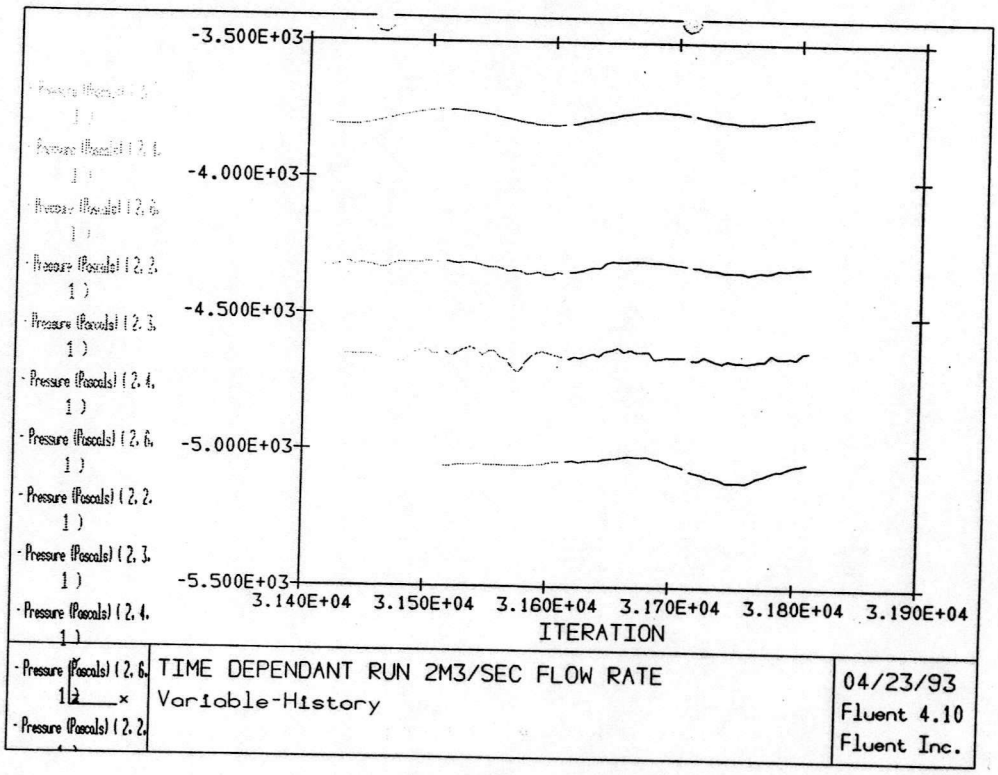

Figure 32 *Inlet Pressure Variable History, NAB214*
(20% design flow, Time Step 0.5 secs, 100 iterations per time step)

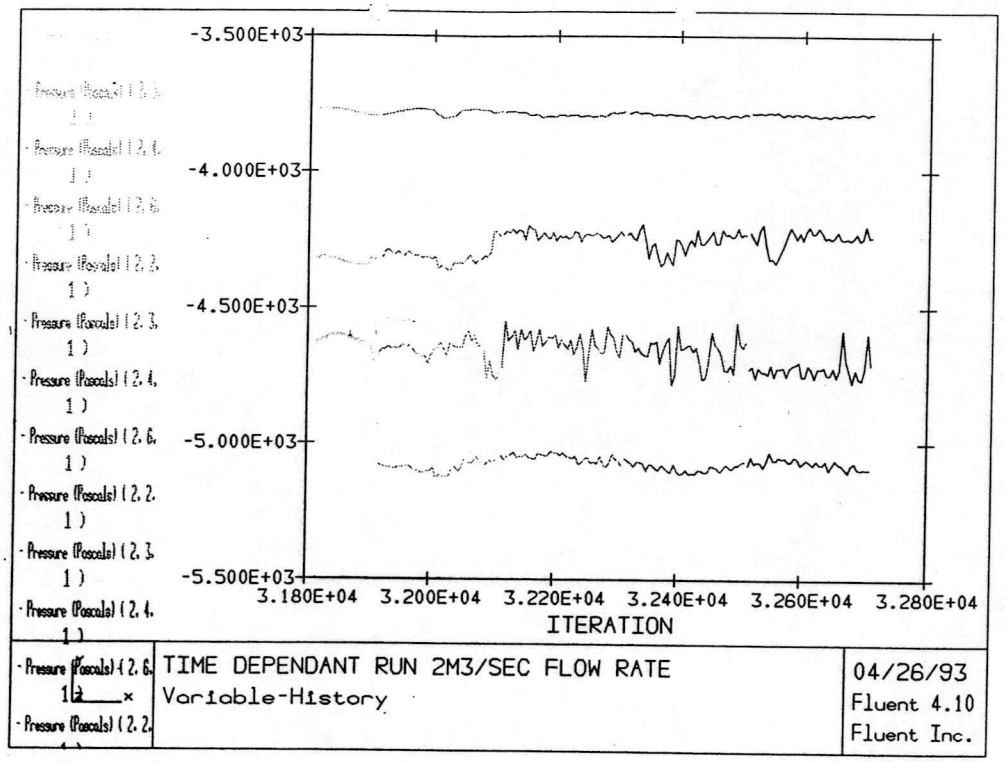

Figure 33 Inlet Pressure Variable History, NAB219
(20% design flow, Time Step 0.04 secs, 200 iterations per time step)

2.2.5 Full Unsteady Euler Solutions

Having now gained a converged solution at several fan duty points for unsteady incompressible flow it was decided to generalise by allowing compressibility, that is , include the energy equation into the formulation. This complication seemed justified as Bosman [1984] suggested that energy transfer may be the key to the formulation of the stall cells. As Bosman's paper was the main motivation behind this investigation, it was decided that this detour would be worth pursuing. The solutions of when the energy equation was used and when is was not, are compared in detail later to highlight any differences.

Initially a steady state compressible run of 2000 iterations was completed for the highly stalled case. This solution acted as the initial data set for subsequent unsteady model runs. The following residuals were noted:

Table 12 Steady State Compressible Flow Residuals

Run Name	Number of iterations	Pressure Residual	U-Velocity Residual	V-Velocity Residual	W-Velocity Residual	Enthalpy Residual
NAB305	2000	1.3×10^{-1}	1×10^{-3}	6×10^{-3}	2×10^{-3}	2×10^{-4}

The time dependent runs below followed

Table 13 Summary of Euler Runs

Run	% of Design Flow	Pressure Residual	U-Velocity Residual	V-Velocity Residual	W-Velocity Residual	Enthalpy Residual	Time Step (secs)	Max No. of iterations	No of time steps
NAB309	20%	1×10^{-1}	6×10^{-4}	5×10^{-3}	2×10^{-3}	2×10^{-4}	0.04	100	8
NAB315	20%	1×10^{-2}	1×10^{-7}	2×10^{-7}	3×10^{-7}	7×10^{-8}	7×10^{-7}	100	8
NAB319	20%	1×10^{-2}	1×10^{-7}	2×10^{-7}	3×10^{-7}	9×10^{-8}	7×10^{-7}	100	8
NAB323	20%	2×10^{-2}	1×10^{-7}	1×10^{-7}	2×10^{-7}	9×10^{-8}	7×10^{-7}	200	4
NAB328C	20%	2×10^{-2}	1×10^{-7}	2×10^{-7}	2×10^{-7}	8×10^{-8}	1×10^{-7}	200	8
NAB333C	20%	3×10^{-2}	1×10^{-7}	2×10^{-7}	2×10^{-7}	8×10^{-8}	1×10^{-7}	200	8
NAB338C	20%	2×10^{-2}	1×10^{-7}	2×10^{-7}	2×10^{-7}	8×10^{-8}	1×10^{-7}	200	20
NAB415C	20%	1×10^{-2}	1×10^{-7}	7×10^{-7}	2×10^{-6}	2×10^{-7}	7×10^{-7}	100	10
NAB505C	20%	8×10^{-2}	6×10^{-8}	1×10^{-7}	2×10^{-7}	4×10^{-8}	1×10^{-8}	100	20
NAB511C	20%	9×10^{-1}	9×10^{-8}	1×10^{-7}	2×10^{-7}	9×10^{-8}	1×10^{-8}	100	20

The first unsteady Euler run, NAB309, was completed with a relatively large time step. This converged, but despite the low flow rate, no unsteadiness was detected. Further reductions in time step to 0.005 sec and $1x10^{-6}$ sec produced unstable results although the latter run was stable for a large portion of the time steps after which it suddenly and unexpectedly diverged. It was only when a tiny time step of $7x10^{-7}$ was used in NAB315, that the formulation became consistently stable. This time step, however, is unpractical as such a large number are required to represent a useful time scale. Whether unsteady effects were present or not, the time of the complete run was just 6 μsec which was too small to differentiate between numerical perturbations and real flow phenomena, even when these runs were extended for further time steps. For interest it was decided to continue the trend of reducing the time step to examine stability. A reduction to $1x10^{-8}$ yielded stable results, but for the reasons mentioned earlier, no stall cell movement could be identified.

2.2.6 Comparisons between Incompressible and Compressible formulations

The differences between the Fluent incompressible and compressible computational model results are discussed here. For completeness, both unsteady and steady-state counterparts are examined. The following four areas are investigated

(a) final residuals
(b) inlet pressure variable histories
(c) predicted fan static pressure rise
(d) meridonial velocity vector plots
(e) solution stability

Each are examined in turn.

2.2.6.a Residuals

Final recorded residuals are tabulated below.

Table 14 Final residual comparisons

Filename	Governing Equations	Pressure Residual	U- Velocity Residual	V-Velocity Residual	W-Velocity Residual
PV11	Steady, Incompressible	$1x10^{-1}$	$8x10^{-4}$	$5x10^{-3}$	$2x10^{-3}$
NAB305	Steady, Compressible	$1x10^{-1}$	$1x10^{-3}$	$6x10^{-3}$	$2x10^{-3}$
NAB219	Unsteady*, Incompressible	$9x10^{-2}$	$8x10^{-4}$	$1x10^{-3}$	$4x10^{-3}$
NAB309	Unsteady*, Compressible	$1x10^{-1}$	$6x10^{-4}$	$5x10^{-3}$	$2x10^{-3}$

* Note: a time step of 0.04 was used.

Before we scrutinise Table 14 the reader should be aware of the following:

(i) Similar time steps have been chosen for the unsteady comparisons, due to the residual sensitivity to time step duration.

(ii) Enthalpy residuals cannot be compared between the compressible and incompressible runs as the energy equation is not solved in the latter cases.

(iii) The recorded residual values, even when the solution has properly converged, do randomly perturb. These perturbations can effect the most significant figure. Therefore the examination should really only concern itself with differences in order of magnitude.

With the above in mind, no substantial differences in error residual were noted.

2.2.6b Inlet Variable History

The same four runs gave similar stochastic pressure history traces. See Figures 34 to 37. When examining these figures the reader should note that the pressures are recorded at inlet to the domain. The upper curves represent the pressure at the duct core: the bottom curves the duct periphery. The time dependent runs show small discontinuities at regular iteration intervals. These breaks are due to the storage of files after every couple of time steps and are not due to some numerical phenomena.. Some differences in the predicted pressure values may be seen in these figures. These will be examined in the next sub section.

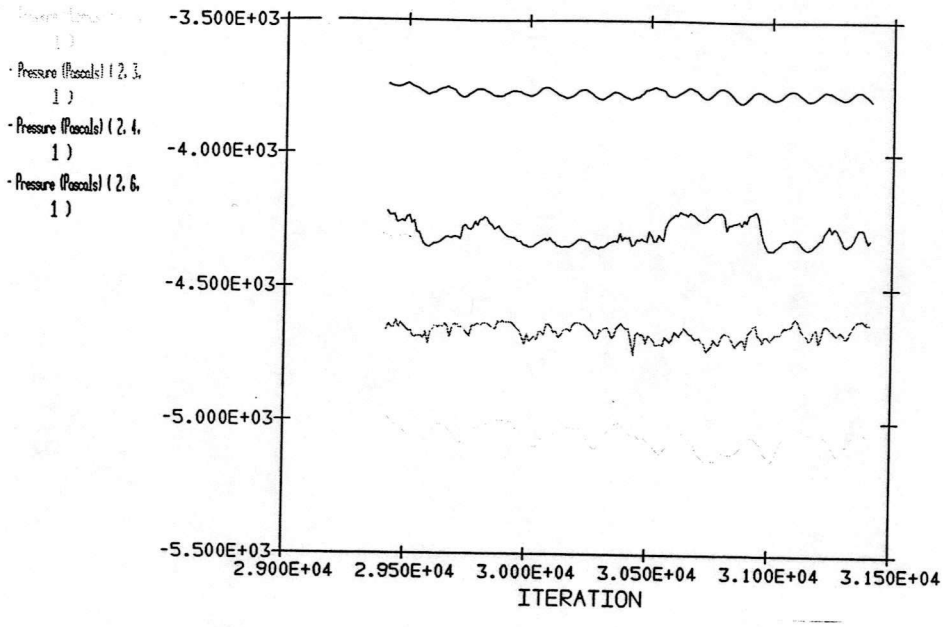

Figure 34 Steady Incompressible Run PV11 Variable History: Inlet Pressure

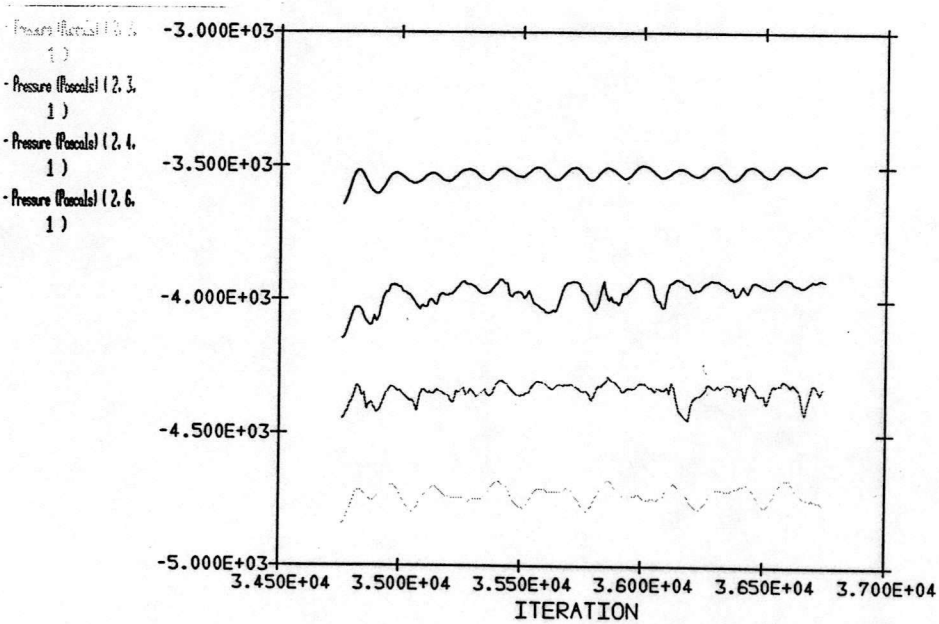

Figure 35 Steady Compressible Run NAB305 Variable History: Inlet Pressure

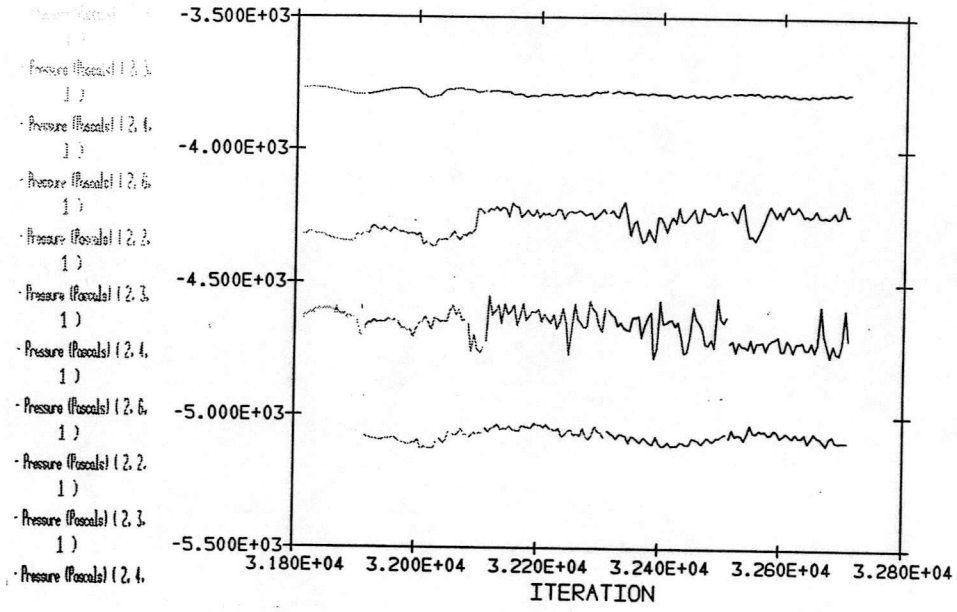

Figure 36 Unsteady Incompressible Run NAB219 Variable History: Inlet Pressure

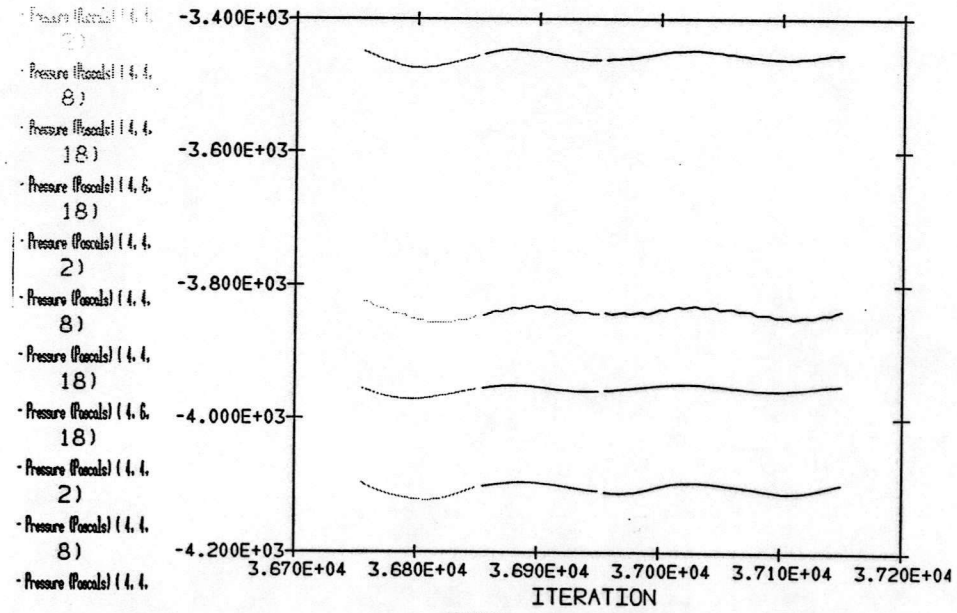

Figure 37 Unsteady Compressible Run NAB309 Variable History: Inlet Pressure

2.2.6c Predicted fan static pressure rise

The fan static pressure rise was calculated using the mass weighting approach of section 2.2.3e, with the addition of a density term when averaging the compressible results.

The results are graphically summarised in Figure 38. The steady-state results for the incompressible and compressible runs are remarkably similar. The unsteady runs are likewise (the reader should note the false scale- the pressure perturbations are relatively small).

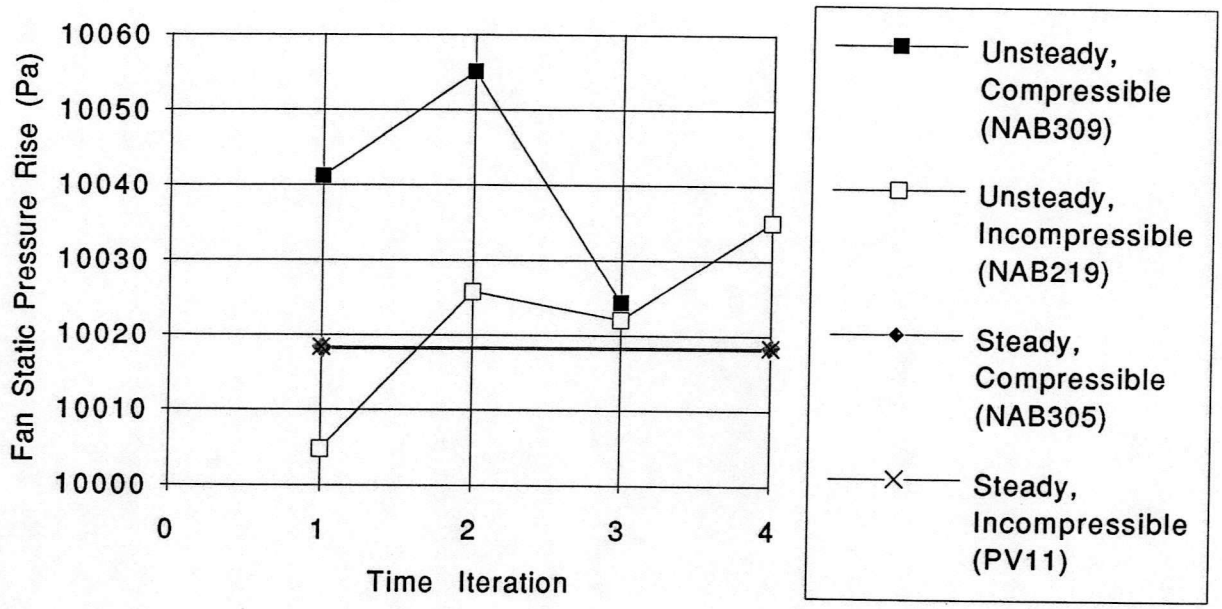

Figure 38 Comparison of Fan Static Pressure Rise Predictions

2.2.6d Solution Stability

The compressible runs were unstable between time steps of 0.04 and $1x10^{-7}$ seconds. The incompressible runs however were unstable and all time steps below 0.04 seconds. For the compressible runs of the smallest time step, some oscillation of pressure at the fan inlet duct was measured. The predicted fan static pressure rise for

these runs is shown in Figure 39. Note the large amplitude of oscillation that cannot correspond the small perturbations seen in Figure 38 for the longer time steps.

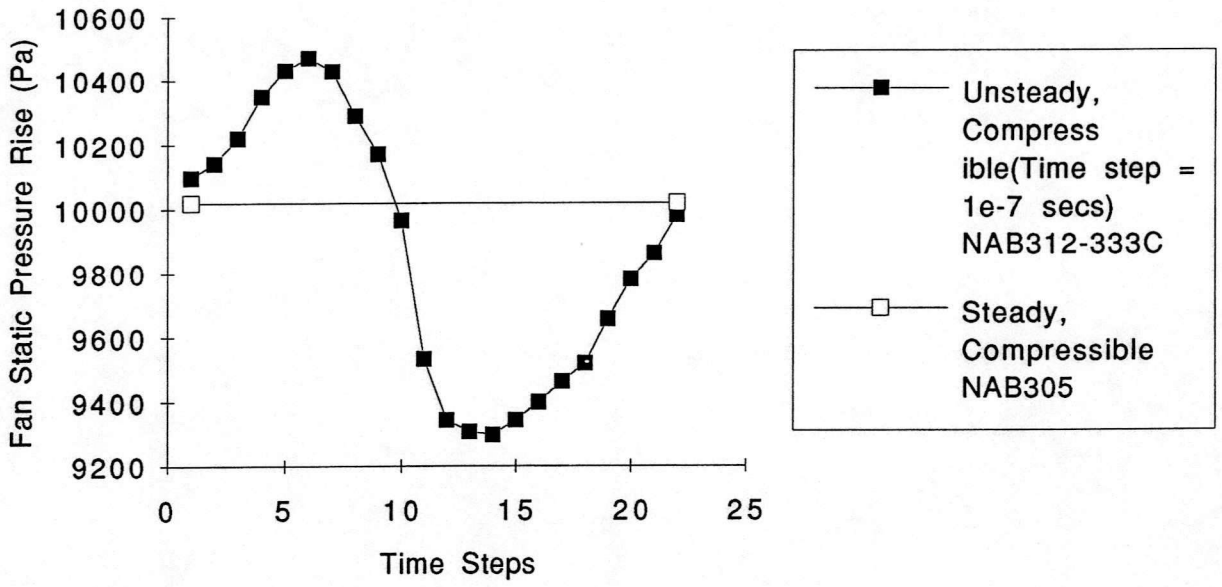

Figure 39 Unsteady oscillatory pressure rise predictions

2.2.6e Meridonial velocity vector plots

These showed no appreciable differences between all those examined.

2.3 The FLUENT Mizuki model

The FLUENT time dependent runs with plagued with instability problems. The incompressible runs became unstable at time steps below $\Delta t = 0.04$ and the compressible runs were only stable out side the band 0.04 to $1x10^{-7}$ seconds. Unfortunately this meant that the time steps necessary to capture rotating stall, of the order 0.001 secs, could not be successfully run. Staff at FLUENT said that the problem physics, that of an highly twisted adverse-pressure flow, was within FLUENT's capabilities. They suggested that the problem was likely be the mesh; both due to distorted cells and flows which were not predominantly normal to one of the cell face directions. With the L3R being a particularly complex model, many compromises in the cell aspect ratios and skewness were made. Together with the inlet ducting and vaneless discharge flow not corresponding to a cell face direction, FLUENT's explanation was feasible. However to fully convince the authors, it was decided to import the Mizuki impeller geometry from PHOENICS into the FLUENT suite and see if it was time-step sensitive. The Mizuki model was considered useful as there were no highly skewed cells or flows that would not generally follow cell local directions.

2.3.1 Problem Set-up

The original PHOENICS BFC (Body fitted co-ordinate) file for the Mizuki impeller was filtered through a small FORTRAN utility, written by the authors, called CONVERT.F77. From here it was imported into FLUENT and the boundary conditions corresponding to incompressible inviscid flow applied. Symmetrical cells were set on blade surfaces and cyclic cells were applied to represent the two-cell vaneless discharge. As per all of the previous cases, a volume flow rate was specified at inlet and a static pressure set at discharge.

2.3.2 Steady State Fluent Mizuki Runs

Before invoking the time dependent option a series of steady state runs, leading to a fully stalled condition, were completed.

Table 15 Steady State Fluent Mizuki Runs: Residuals

Filename	Flow Coefficient	Number of Iterations	Pressure Residual	U-Velocity Residual	V-Velocity Residual	W-Velocity Residual
FMIZ2	0.4	250	$6x10^{-4}$	$1x10^{-4}$	$2x10^{-4}$	$1x10^{-4}$
FMIZ5	0.4	1000	$4x10^{-4}$	$6x10^{-5}$	$4x10^{-5}$	$1x10^{-4}$
FMIZ11	0.2	500	$2x10^{-4}$	$6x10^{-5}$	$6x10^{-5}$	$3x10^{-4}$
FMIZ21	0.1	1000	$6x10^{-3}$	$4x10^{-3}$	$2x10^{-3}$	$4x10^{-3}$

All of the FLUENT Mizuki runs were completed with the following relaxation parameters:

Table 16 Fluent Mizuki Model Relaxation Parameters

Variable	Relaxation	Number of Sweeps
Pressure	0.1	10
Velocity	0.3	3

The first run completed was FMIZ2. After patching on a velocity field equal to the inlet velocity, throughout the computational domain, the solution converged in 250 iterations. In addition, the reader should note that the run was prematurely halted after 250 of the proposed 500 iteration run by FLUENT. The residuals had reached a summated value of $1x10^{-3}$: at this default value FLUENT assumed that the equations had converged. This level of convergence had never been achieved for the L3R model. At this point it is also worth recollecting that to get the L3R model to what was regarded as converged required a series of runs from low to high speed, which used thousands of iterations. Here it was managed in 250 and is one step. For interest it was decided, after resetting the FLUENT default residual convergence parameter, to continue the run to see if the solution would converge any further. After 1000 iteration no benefits were noted.

With a good approximation to the flow from FMIZ2, it was decided to proceed to the below design flow cases . Two runs were completed with flow coefficients of Ψ=0.2 and 0.1, the latter representing stalled flow operation. The mid-channel velocity vector plot for the Ψ=0.1 case is shown in Figure 38.

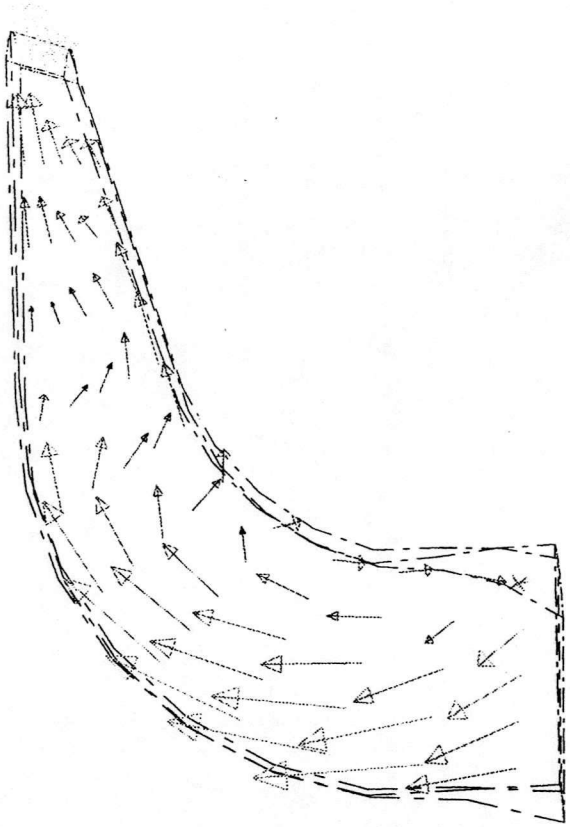

Figure 38 Fluent Mizuki Highly Stalled Flow Meridonial Mid-Channel Velocities

2.3.3 Unsteady Fluent Mizuki Runs

As a first step it was decided to investigate the sensitivity of the model to time step. This analysis could be done interactively due the relatively small number of computational cells and hence reasonable run times. The stalled condition of Ψ=0.1 modelled by FMIZ21 was used as the starting data set in all time dependent runs.
The results from these runs are tabulated below. All runs were completed over one time step (with max. 100 iterations) as this was all that was required to determine stability (in the earlier L3R runs instability was noted by a divergence within only a few iterations).

Table 17 Interactive Time Dependent Runs

Time step	Pressure Residual	U-Velocity Residual	V-Velocity Residual	W-Velocity Residual
$4x10^{-2}$	$1x10^{-2}$	$3x10^{-3}$	$2x10^{-3}$	$4x10^{-3}$
$4x10^{-3}$	$8x10^{-3}$	$3x10^{-3}$	$2x10^{-3}$	$3x10^{-3}$
$4x10^{-4}$	$1x10^{-3}$	$4x10^{-4}$	$4x10^{-4}$	$7x10^{-4}$
$4x10^{-5}$	$4x10^{-4}$	$3x10^{-4}$	$1x10^{-4}$	$1x10^{-4}$
$4x10^{-6}$	$3x10^{-5}$	$4x10^{-5}$	$2x10^{-5}$	$2x10^{-5}$
$4x10^{-7}$	$2x10^{-5}$	$3x10^{-5}$	$8x10^{-6}$	$1x10^{-5}$
$4x10^{-8}$	$8x10^{-6}$	$1x10^{-5}$	$2x10^{-6}$	$3x10^{-6}$

All runs were therefore stable, with a distinctive trend of decreasing residual with respect to time step duration.

Two batch runs were subsequently completed, keeping all solution parameters constant. These were

Table 18 Batch Time Dependent Runs

Filename	Time Step	Pressure Residual	U-Velocity Residual	U-Velocity Residual	U-Velocity Residual	Max. No. of Iters Per Time Step	Number of Time Steps
PMIZ35	0.04	$1x10^{-2}$	$3x10^{-3}$	$2x10^{-3}$	$4x10^{-3}$	100	20
PMIZ45	$2.5x10^{-4}$	$3x10^{-3}$	$8x10^{-4}$	$6x10^{-4}$	$1x10^{-3}$	100	20

Non of the random perturbations, as seen in the L3R unsteady investigations, were detected here. Figures 39 and 40, taken from PMIZ45, demonstrate how smooth the output was. Incidentally the tiny step for this run is a tenth of the time for a stall cell to pass across a blade passage, representing a desirable time step for stall cell numerical computation.

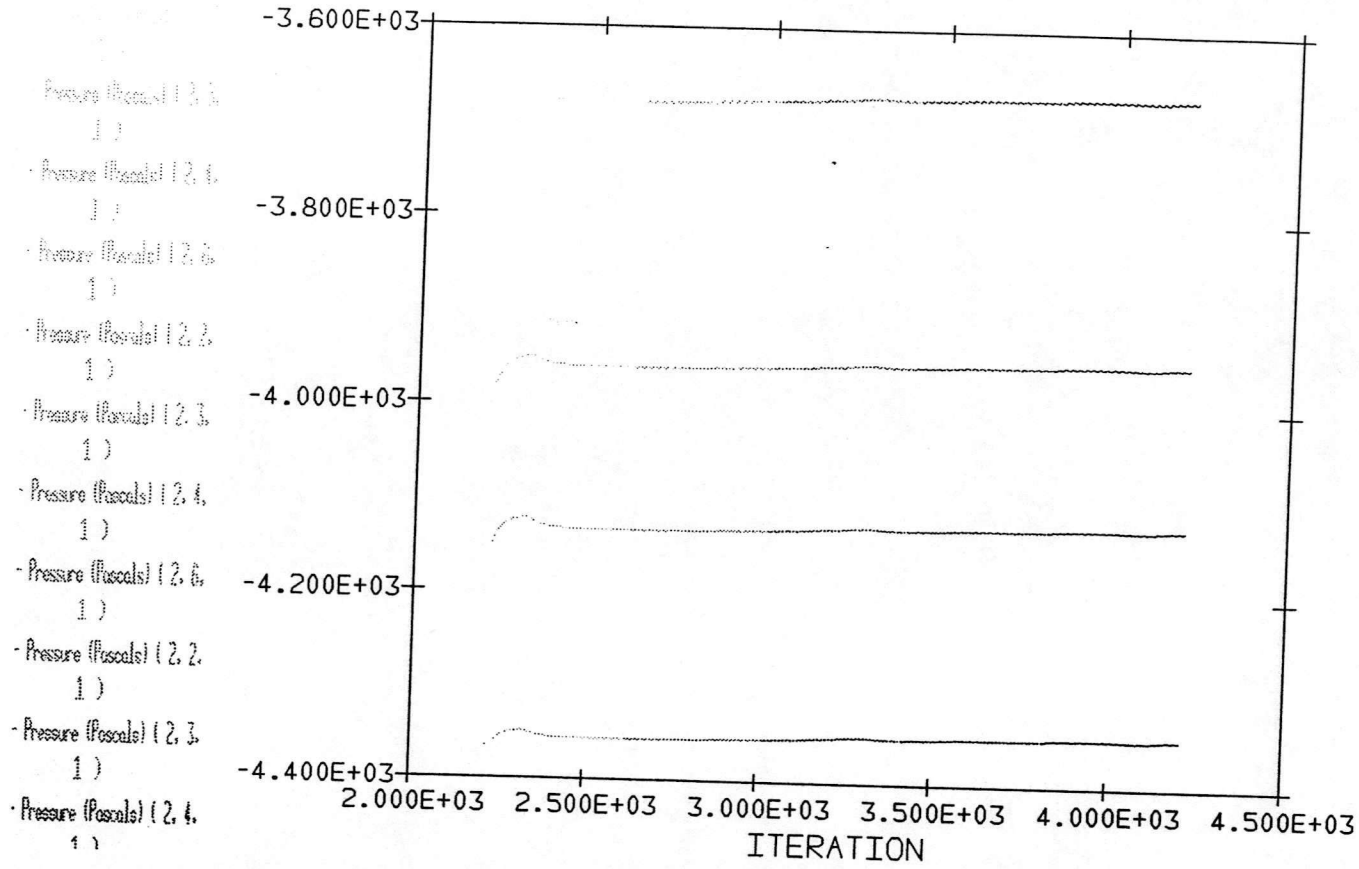

Figure 39 Pressure History at Inlet to Mizuki Impeller Passage

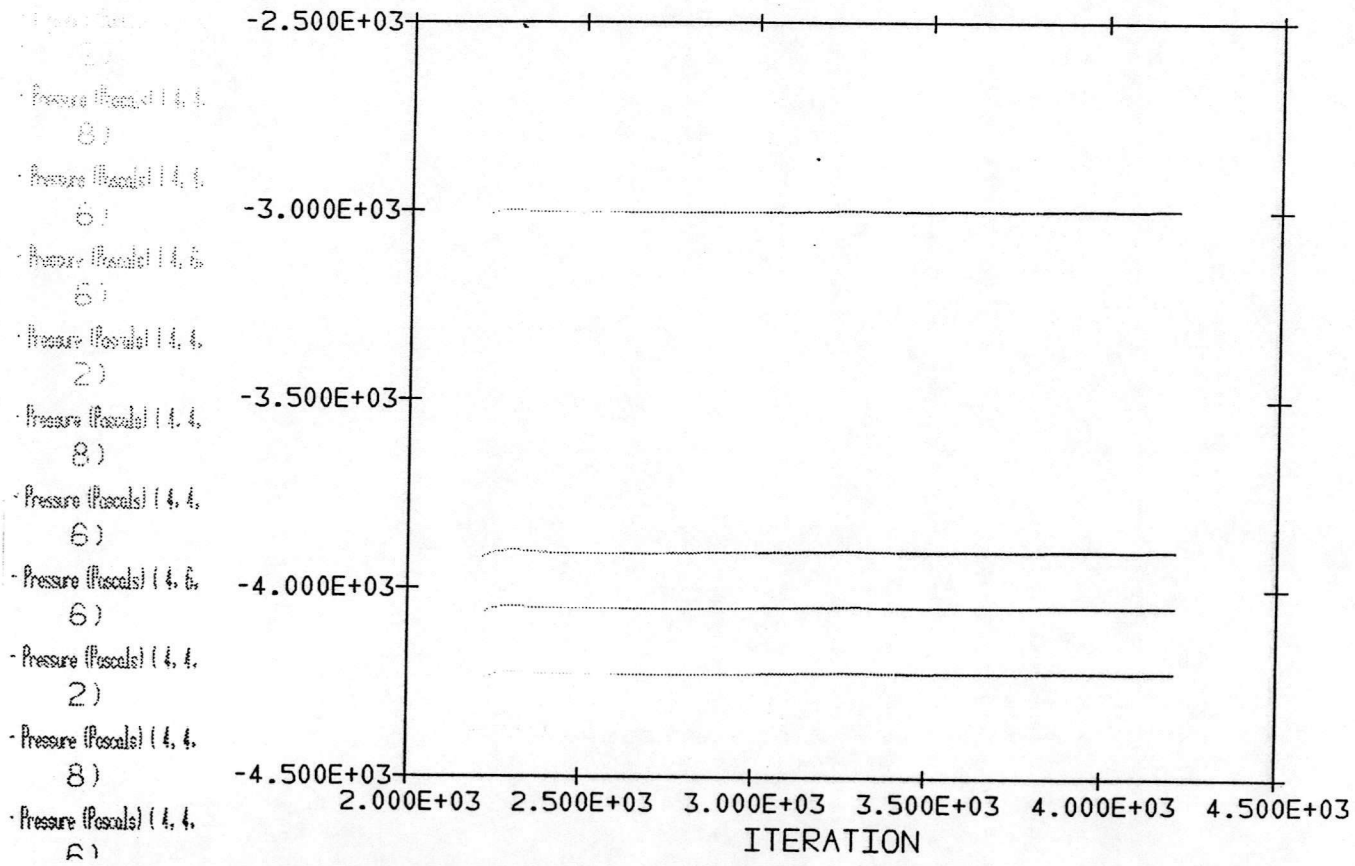

Figure 40 Pressure History within Mizuki Impeller Passage

3. Conclusions

a) Using a fully 3 dimensional incompressible steady-state formulation of the inviscid Euler Equations, large recirculating regions of stalled flow have been predicted. The location of these cells has not been verified here against experimental measurements, but have been shown to appear only at flow rates corresponding to fan stall. Therefore it is expected that an inviscid model could be used to predict the volume flow fate at which a fan stalls.

b) The SIMPLE solution algorithm used by FLUENT has shown to be sensitive to both the fan operating conditions and time-step duration. It has been demonstrated that careful quasi-equilibrium changes in fan operating condition may be used to great effect to stabilise the equations.

c) Predictions of fan pressure rise using an inviscid formulation do not differ with respect to volume flow. Inviscid flow models should only be used for gross flow assessment.

d) The Mizuki and Bladeless L3R models demonstrate that an inlet mesh dimension of 5 x 5 is sufficient to predict recirculation.

e) No unsteady field variable perturbations, characteristic of stall were noted when solving the Unsteady Euler equations for a fan operating at very low flow rates.

f) The SIMPLE algorithm has been show to be sensitive to computation mesh cell aspect ratios and skew cells. Very careful consideration should be made before incorporating highly distorted cells into a model.

g) The SIMPLE algorithm, with careful consideration given to computational mesh, may be used to model the flow within turbomachinery passages. In particular, the time dependency option may be invoked so as to sample the flow regime at a frequency corresponding to rotating stall. It would seem at this stage that FLUENT is suitable for predicting rotating stall in a multi-blade model.

4. Further Work

a) Multiple blade passage runs should now be completed.

b) It would be interesting to see if the introduction of a turbulent viscosity model would improve fan pressure rise predictions.

References

Adler, D.
"Status of Centrifugal Impeller Internal Aerodynamics: Part 1: Inviscid Flow Prediction Methods"
ASME Journal Of Engineering For Power Vol. 102 pp 728-737
July 1980

Bennett, I. and Vezza, M.
"Review- Centrifugal Fan Experiments and Prediction"
G.U. Aero Report No. 9203
Dept. of Aerospace Engineering
University of Glasgow
Jan. 1992

Bennett, I. and Watson, H.
"Single Inlet L3R Fan"
Report A436
James Howden Group Technology
Old Govan Road
Renfrew PA4 0XJ

Bosman, C. and Ahrabian, D.
"Calculation of Stalled flow in a Centrifugal Impeller"
IMechE Conference: Computational Methods for Turbomachinery
Paper No C67/84 pp173-182
1984

BS848: Part 1: 1980
British Standards Institute

Edwards, J.P., Glynn, D.R. and Tatchell, D.G.
"Flow and Blade Loading in Centrifugal Impellers"
First International Phoenics Users Conference, 1985
CHAM Ltd
40 High Street
Wimbledon
London SW19 SAU

Hirsch, C.
"Numerical Computation of internal and External Flows. Vol. 1: Fundamentals of Numerical Discretization"
Wiley-Interscience Publication
John Wiley and Sons
Chichester, England 1990

Mizuki, S., Ariga, I. and Watanabe, I.
"Investigation Concerning the Blade Loading of Centrifugal Impellers"
ASME Gas Turbine Conference Paper 74-GT-143, 1974

Soundra-Nayagam, M.,Bolton, N. and Chen, P.
"The Prediction and Detection of Unstable Flows in Power Station Fans"
Proc IMechE, Int Conf on power Station Pumps and Fans, London
May 1992

Stanitz, J.D.
"Two Dimensional Compressible Flow in Conical Mixed Flow Compressors"
NACA TN 1744
1948